Strehlow, K., Gottsmann, J., Rust, A., Hautmann, S., & Hemmings, B. (2020). The influence of long- and short-term volcanic strain on aquifer pressure: a case study from Soufrière Hills Volcano, Montserrat (W.I.). *Geophysical Journal International*, *223*(2), 1288–1303. https://doi.org/10.1093/gji/ggaa354

The influence of long- and short-term volcanic strain on aquifer pressure: a case study from Soufrière Hills Volcano, Montserrat (W.I.)

K. Strehlow[1,a], J. Gottsmann[2,b], A. Rust[2,c], S. Hautmann[3,d] and B. Hemmings[4,e]

[1]GEOMAR Helmholtz Centre for Ocean Research Kiel, Germany. [2]School of Earth Sciences, University of Bristol, UK. [3]Department of Earth Sciences, ETH Zürich, Switzerland. [4]GNS Science, Wellington, New Zealand.

[a]kstrehlow@geomar.de; [b]J.Gottsmann@bristol.ac.uk; [c]Alison.Rust@bristol.ac.uk; [d]stefanie.hautmann@googlemail.com; [e]b.hemmings@gns.cri.nz

Accepted date; Received date; in original form date

Abbreviated title: Water level changes caused by volcanic activity on Montserrat

Corresponding author: Karen Strehlow (kstrehlow@geomar.de, Tel. +49 431 6002568)

Summary

Aquifers are poroelastic bodies that respond to strain by changes in pore pressure. Crustal deformation due to volcanic processes induces pore pressure variations that are mirrored in well water levels. Here, we investigate water level changes in the Belham valley on Montserrat over the course of two years (2004-2006). Using finite element analysis, we simulate crustal deformation due to different volcanic strain sources and the dynamic poroelastic aquifer response. While some additional hydrological drivers cannot be excluded, we suggest that a poroelastic strain response of the aquifer system in the Belham valley is a possible explanation for the observed water level changes. According to our simulations, the shallow Belham aquifer responds to a steadily increasing sediment load due to repeated lahar sedimentation in the valley with rising aquifer pressures. A wholesale dome collapse in May 2006 on the other hand induced dilatational strain and thereby a short-term water level drop in a deeper-seated aquifer, which caused groundwater leakage from the Belham aquifer and thereby induced a delayed water level fall in the wells. The system thus responded to both gradual and rapid transient strain associated with the eruption of Soufrière Hills Volcano (Montserrat).

This case study gives field evidence for theoretical predictions on volcanic drivers behind hydrological transients, demonstrating the potential of hydrological data for volcano monitoring. Interrogation of such data can provide valuable constraints on stress evolution in volcanic systems and therefore complement other monitoring systems. The presented models and inferred results are conceptually applicable to volcanic areas worldwide.

Keywords: Hydrology, Numerical modelling, Volcano monitoring, Fracture and flow, Permeability and porosity, Transient deformation

Acknowledgements

Author contribution: KS planned and conducted the research, with input and supervision from JG and AR; SH provided input regarding strain measurements on Montserrat; BH provided data and insights concerning the hydrological system on Montserrat; KS drafted the initial version of the manuscript, which has been reviewed and approved by all authors. The authors would like to acknowledge Steve Ingebritsen, Jenni Barclay, Marc Dumont and two anonymous reviewers, whose reviews led to a significant improvement of the paper. The research leading to these results has received funding from the People Programme (Marie Curie Actions) of the European Union's Seventh Framework Programme (FP7/2007-2013) under the project NEMOH, REA grant agreement number 289976. KS acknowledges funding from the project MED-SUV, under grant agreement number 308665, also part of the European Union's Seventh Framework Programme. JG acknowledges funding from the Royal Society (UF090006), the Natural Environment Research Council (NE/E007961/1) and the EC (FP7-ENV-2011: "VUELCO"28276). SH acknowledges funding from the Swiss National Science Foundation (PMPDP2_158309) and the National Geographic Society (GEFNE34-12). The authors would like to acknowledge Montserrat Utilities and Bill Tonge for providing their well level and precipitation data, as well as Karen Pascal (part of the Montserrat Volcano Observatory, funded by the UWI Seismic Research Centre) and the Government of Montserrat for sharing mean sea level pressure data.

1 Introduction

Hydrological systems can respond to or modify the expression of magmatic processes or become an agent of volcanic unrest themselves, resulting in observable transients in volcano and hydrological monitoring systems (e.g., Rouwet et al., 2014, Newhall et al., 2001, Jasim et al., 2018). If we understand the underlying mechanisms, we can integrate hydrological observations with other volcano monitoring systems to get a more complete picture of volcanic processes and related hazards and their interactions with the local hydrology.

Changes in water levels in wells, springs, and lakes have been reported in association with eruptions at many volcanoes of different kinds and in various settings (e.g. Newhall et al., 2001, and references therein). Several volcanic drivers have been proposed as causes for these changes, including the injection of fluids derived from magmatic degassing into the aquifer (Capasso et al., 2014) or changes in groundwater flow patterns e.g. through the opening and closure of fractures (Hautmann et al., 2010, Hurwitz and Johnston, 2003).

An often-proposed mechanism behind changes in well water levels are strain-induced changes in pore pressure. Aquifers are poroelastic media, i.e. the solid matrix behaves elastically, but is coupled to the pore fluid and its flow. Poroelastic media react to applied volumetric strain like a confined sponge: pore pressure rises under compression and falls during dilatation owing to the decrease and increase in pore space, respectively (Wang, 2000). Conversely, the presence of pore fluids also affects the deformation of the solid matrix and variations in pore pressure deform the surrounding matrix (Wang, 2000). Changes in water levels due to pore pressure changes resulting from seismic strains before, during or after earthquakes have been widely observed (e.g. Roeloffs, 1996, Shibata et al., 2010, Kopylova and Boldina, 2012, Takahashi et al., 2012, Brodsky et al., 2003).

Previous work on poroelastic processes at volcanoes almost exclusively considered ground deformation induced by pressure changes in hydrothermal systems, a process commonly studied with one-way coupled numerical models (e.g. Todesco et al., 2004, Fournier and Chardot, 2012, Coco et al., 2016). Less studied are poroelastic responses of aquifers to volcanic processes such as reservoir pressure changes, which frequently cause stress changes in the surrounding crust. Some attempts at interpreting pre-, syn- and post-eruptive water level changes in the light of volcanic strain have been performed for example at Usu and Meakan-dake volcano in Japan (e.g. Yokoyama and Seino, 2000, Takahashi et al., 2012) and Krafla volcano in Iceland (Stefansson, 1981). By tracing water level changes in response to known strain excitations, the strain sensitivity, i.e. the well level change per unit applied strain, of an aquifer can be quantified. This method is common in studies of seismically-induced water level changes and was applied by several volcanological studies (e.g. Matsumoto et al., 2002, Kopylova and Boldina, 2012, Shibata et al., 2010) in order to derive crustal strain from observed strain-induced water level changes.

Only a few, very simple poroelastic problems have been solved analytically, for example the compression of a homogeneous, water-saturated block (e.g. Rice and Cleary, 1976). For more complex problems, e.g. with heterogeneous media and/or more sophisticated deformation sources, and for the investigation of time-dependent fluid-flow effects, a numerical approach is necessary. Strehlow et al. (2016) present the first fully-coupled, time-dependent numerical models for poroelastic water level changes at volcanoes. Using finite element analysis, they simulate crustal deformation accompanying magma chamber pressurization and the resulting significant hydraulic head changes as well as flow through the porous aquifer.

Following the theoretical analysis of Strehlow et al (2016) that includes a detailed sensitivity analysis, this paper provides the first step towards application of these models in

volcano monitoring. After an introduction to the study site, i.e. the island of Montserrat, West Indies, and its volcanological and hydrological system, we report volcanic activity and observed water level changes in 2004-2006. This period was chosen as the focus of this study since both hydrological and volcano monitoring data are available, and the time frame covers an intra-eruptive quiescent period from July 2003 to July 2005, the renewal of lava extrusion in August 2005 and the formation and partial explosive destruction of a new dome (Odbert et al., 2014a). We suggest that these water level variations are caused by volcanic strain and present results of numerical models that are applied to test our hypotheses. Limits and implications of these results are discussed, and we finally conclude that well level changes on Montserrat are indeed at least strongly affected by volcanic processes acting on different time-scales.

2 Setting

2.1 Geology of Montserrat

Montserrat is a small (sized 16 km x10 km) volcanic island located in the north of the Lesser Antilles inner volcanic arc (Fig. 1). The island consists of three volcanic centres that decrease in age from north to south, i.e., from the extinct Silver Hills and Centre Hills to the youngest Soufrière Hills Volcano.

The northernmost volcanic complex Silver Hills (SH) was active 2.6 to 1.2 million years ago, while the Centre Hills (CH) were erupting about 950 to 550k years ago (Harford et al., 2002). The remnants of the old andesitic volcanic domes from the extinct volcanic centres SH and CH are today dominating surface expressions on the island. Their flanks are surrounded by aprons of volcaniclastics, which are predominantly pyroclastic flow deposits, with lesser amounts of pumice-and-ash-flow, pumice-fall, lahar, debris-avalanche and fluvial deposits (Shalev et al., 2010;

Hautmann et al., 2013). The volcaniclastic beds are intersected by radially incised valleys that are formed by run-off from heavy rainfall (Hemmings et al., 2015a).

The active Soufrière Hills Volcano (SHV) in the south of Montserrat is an andesitic dome-building volcano that first started erupting 175k years ago (Harford et al., 2002). After an approximately 370 years period of dormancy (Kokelaar, 2002), renewed activity began in 1995. Since then, SHV has undergone various cycles of lava dome extrusions and discrete Vulcanian explosions alternating with phases of volcanic quiescence and cessation of dome growth (i.e., Odbert et al., 2014b). Episodes of surface activity are typically related with ground deflation, while periods of quiescence are associated with a re-pressurization of the subsurface magmatic system and a consequent ground inflation. After a partial dome collapse in 2010, which marked the last major activity to date, the volcano entered a new episode of continuous surface inflation that is still ongoing at time of this writing.

The two volcanic complexes CH and SHV are geologically separated by the ESE trending Belham Valley fault (BVF). The BVF is part of a larger fracture system that connects the Bouillante-Montserrat graben between Guadeloupe and Montserrat in the east with the Montserrat-Havers Fault System that extends to the west of Montserrat (Feuillet et al., 2010). The fault appears to be currently inactive: there is an absence of earthquakes in the historic record and repeated electronic distance measurements indicate a lack of movements along the fault (MVO, pers. comm.). The Belham Valley, which is the morphological expression of the BVF, is a major drainage channel that has been filled with >12 m lahar and pyroclastic deposits since the beginning of the SHV eruption (Froude, 2015).

2.2 The SHV magmatic system

153 The analysis of geodetic data from different volcanic activity phases of SHV allowed for
154 the identification and characterization of three connected pressure sources in the crust (e.g. Odbert
155 et al., 2014b). Assembling these inferred sources gives a model of a magma plumbing system that
156 consists of two vertically-stacked magma chambers that link to the surface via a dyke-conduit
157 feeder system (i.e., Hautmann et al., 2013, 2014). The lower magma chamber (LMC) has been
158 found to be prolate with its centroidal source depth located at ~13 km bsl (Hautmann et al., 2010),
159 while the upper magma chamber (UMC) has been inferred to be spherical, centred at ~6 km depth
160 (Voight et al., 2006). Independent studies on magma flow dynamics, seismic tomography and
161 strain data inversion constrained the UMC:LMC magma chamber volume ratio to 1:3, whereof the
162 LMC is estimated to have a size of 8 km^3 (Paulatto et al., 2012; Hautmann et al., 2013; Melnik and
163 Costa, 2014). A NW-SE trending dyke that opens at ~1 - 1.5 km depth into a small cylindrical
164 conduit connects the UMC with the surface (Mattioli et al., 1998; Costa et al., 2007; Hautmann et
165 al., 2009; Linde et al., 2010; Gottsmann et al., 2011).

166 2.3 Hydrology and the Belham aquifer

167 The hydrological system of Montserrat is characterized by high-yielding springs on the
168 upper flanks of the extinct CH and low-lying coastal aquifers in the volcaniclastic aprons
169 (Hemmings et al., 2015a). High infiltration rates limit the surface run-off on Montserrat and
170 streams exist only during and shortly after intense rainfall events, when water flows through deep
171 valleys towards the sea. Rainfall occurs throughout the year but follows a clear seasonality. The
172 wet season ranges from July to November with the highest precipitation values in September to
173 November, and the dry season spans from February to April (Hemmings et al., 2015a). Even
174 though infiltration rates are high, high rates of interception and evapotranspiration significantly
175 reduce the percentage of precipitation that reaches the ground to recharge. Additionally, there is

significant run-off during the very large rainfall events, which further limits recharge. Hemmings et al. (2015a) predict an annual recharge of 10–20% of annual rainfall with a pronounced seasonality, as 70% of the island's recharge occurs between July and December. Recharge rates vary significantly both temporally and spatially. Transpiration is especially high in the forested areas, which limits recharge, while infiltration and recharge rates are high on fresh volcanic deposits (Hemmings et al., 2015a). Simulated estimates of mean (whole island) recharge rates for individual months range from 7.2 (June) to 55.8 mm/month (October) for the whole island, increasing to 217 mm/month in the southern part of the island (Hemmings et al., 2015a).

The Belham valley is the broadest drainage channel on the island with a catchment area of about 16 km^2 (Froude, 2015). It hosts a confined aquifer in reworked gravels and alluvial deposits at depths between 15 and 38 m below sea level (bsl) (Hemmings et al., 2015a) (hereafter called the "Belham aquifer"). Hemmings et al. (2015a, 2015b) also propose a second, deeper and warmer aquifer that feeds the springs of Centre Hills and the Belham aquifer by upflow through a fault and fracture network. The Belham aquifer is confined by a thin cap (about 1 m) of low permeability clay and covered by several meters of lahar deposits. In 2003, previously existing wells, drilled for groundwater development in the Belham valley, were buried and lost under fill accumulations from lahars. In order to regain back-up water supply, HydroSource Associates drilled three new wells in 2004 down to depths of 79 m below ground surface (bgs) (MBV 1), 59 m bgs (MBV 2) and 110 m bgs (test well), respectively (HydroSource 2004). The test well is a pure observation well, while MBV 1 and MBV 2 serve as backup water sources, but are not normally pumped for supply purposes and never pumped during periods of heightened volcanic activity. All wells are hydraulically connected, evidenced by pumping tests conducted by HydroSource Associates. These tests also revealed that the tapped Belham aquifer is highly permeable (10^{-10} m^2)

(HydroSource, 2004). The water is comparatively warm (31° C) and the aquifer is somewhat buffered from atmospheric and seasonal fluctuations in recharge (Hemmings et al., 2015b), although the spatial and temporal uncertainties regarding recharge are significant and preclude well-founded statements regarding the influence of recharge on the wells. In 2012, we operated a continuously recording pressure logger (sample frequency 0.003 Hz) in the test well of Belham valley (see online resource 1), which allows the investigation of possible short-term effects in the aquifer. These data show that the tidal signal in the aquifer is smaller than the general noise in the data. Tidal responses can only cause hydraulic head changes < 0.5 cm and were therefore neglected in this study. Comparison with rainfall data showed furthermore that the system is largely buffered from short-term meteoric events.

3 Observations 2004 - 2006

3.1. Aquifer head changes

The focus of this study is the analysis, modelling and interpretation of water level data recorded between November 2004 and December 2006 in the three wells tapping the Belham aquifer. Provided that weather conditions and volcanic activity allowed access to the valley, water levels in the wells were measured with a portable tape dipper on a roughly weekly basis, with only a single larger gap in the data, between 14th of June and 10th of August 2005. The recorded water level changes (Fig. 2a) indicate three features:

(i) Between November 2004 and May 2006 there is an annual periodicity with a pronounced increase of water levels (0.4 - 0.8 m) between October and March and a slight decrease (~10 cm) of water levels during the summer months.

(ii) Over the entire observation episode, water levels increased by almost 2 m. Particularly after May 2006, this increase follows a general linear trend and even swamps the yearly periodic signal. This increase seems to have continued in some form after the observation period, because one of the wells became flowing artesian in 2011 and has been discharging water into the valley until (at least) 2014 (Hemmings et al. 2015a; Hemmings et al. 2012).

(iii) A notable decrease in water levels by 10 cm is documented between the 25th and 31st of May 2006. Occasionally, one of the three wells shows a short deviation from the overall trend but the decrease at the end of May 2006 is the only short-term signal visible in all three wells. We therefore assume it to be a real effect even though the water level fall is based on just one data point in time.

The Belham aquifer was saturated during the whole period of observations: using the initial depth to water level in the wells (between 3.2 m at MBV2 and 6.63 m at the test well) and the elevation of the wells (about 40 m asl), we can infer that the well water levels were always well above the upper boundary (38 m bsl) of the aquifer.

3.2. Barometric pressures and rainfall

Barometric pressure variations affect well water levels in a complex way and the barometric efficiency and its variation with time depend on aquifer properties and hydrological conditions. The general observation is that in response to an atmospheric pressure drop, well levels rise and vice versa (Rojstaczer and Agnew 1989; Rasmussen and Crawford 1997). We therefore compare the hydrologic data with mean sea level pressure changes (Fig. 2b) that were recorded simultaneously at Montserrat's airport (168 m asl), which is located between SH and CH (data provided by Karen Pascal, owned by the Government of Montserrat). Monthly averaged mean sea level pressures generally display an annual depression between September and November,

correlating with the months with highest precipitation values. Rainfall data collected during the same time interval by the Montserrat Utilities at the Hope rain gauge document the seasonality typical for Montserrat, with largest precipitation values between September and November (Fig. 2b).

In order to test the relation between meteorological parameters and the water levels in the Belham valley, we calculated correlation coefficients of the different data sets, which are shown in Table 1. Cumulative precipitation and monthly averaged mean sea level pressure (before May 2006) both show a good correlation with the well water level. Daily measured precipitation and mean sea level pressure data do not correlate with water levels.

3.3 Volcanic activity

The studied monitoring window was characterized by a switch in volcanic activity from magma chamber inflation and dome-growth cessation (representing the second pause since the beginning of the eruption in 1995) to magma chamber deflation and lava extrusion at the surface (activity episode 3 since 1995). The pause of volcanic activity began in July 2003 after a major dome collapse at SHV and ended in April 2005 with the onset of a series of phreatic and later Vulcanian eruptions, which were precursory to the beginning of a new dome growth phase in August 2005 (Wadge et al., 2014). Since then, the lava extrusion rate increased exponentially (Fig. 2a) until a major collapse on 20th May 2006 removed all dome material that was extruded in Activity Phase 3 and remnants of the earlier Activity Phase 2. The collapse lasted 3 h and involved a total volume of 97×10^6 m^3 (dense rock equivalent) (Wadge et al., 2014). The May 2006 collapse was in its mechanisms (direction, related surges, explosions) similar to the major collapse in July 2003, which marked the end of Activity Phase 2, but the May 2006 event was smaller by a factor of 2

with regard to dome volume removal (Voight et al., 2006). Dome growth resumed subsequently after the collapse in May 2006 and remained steady at a high rate until early 2007.

4 Hypotheses

We propose that the observed water level changes in the Belham aquifer can be caused, or are at least heavily affected, by volcanic processes that induce both long-term and short-term stress changes leading to poroelastic pore pressure changes in the aquifer. This study focuses on the investigation of the aquifer response to volcanic strain and demonstrates that this is an essential component of the drivers behind observed water level changes. This does not rule out the potential contribution of purely hydrological mechanisms (e.g. hydrological recharge and barometric responses) to observed water level signals, although these are ignored in the simulations.

Regarding the potential barometric contributions to water level signals, according to Freeze and Cherry (1979), barometric efficiency of confined aquifers usually falls in the range of -0.2 to -0.8 cm/mbar. During the observation period, the day-to-day variation in mean sea level pressure on Montserrat was less than 5 mbar (Fig. 2b), which translates into water level changes between 1 and 4 cm. We can dismiss atmospheric pressure changes as a cause for the long-term water level increase of about 2 m. The short-term water level fall would require a short-lived, high pressure weather system on 31 May 2006, which cannot be seen in the mean sea level pressure data set, and thus this abrupt water-level change also cannot be attributed to an atmospheric pressure response. Although atmospheric pressure follows a seasonal trend and thus might play a role in the observed periodicity of the water levels, the seasonal signal in the water level data is significantly larger than the expected response to atmospheric pressure variations.

289 Estimation of the potential contribution from recharge variations is less straight-forward.
290 Recharge in the Belham valley is seasonal and may thus contribute to the seasonal signal in the
291 water level data. Climate-driven seasonal and interannual recharge variations on Montserrat are
292 also potentially coupled with recharge changes induced by the destruction of vegetation (and
293 therefore, transpiration potential) by volcanic activity (Hemmings et al 2015a). While precipitation
294 did not significantly change (Fig. 2b), recharge modelling by Hemmings et al. (2015a) showed
295 that, due to lower evapotranspiration and higher infiltration rates, recharge on Montserrat is almost
296 5 times higher on bare soils and fresh volcanic deposits than on forested regions. Due to the intense
297 volcanic activity of the last 20 years, vegetation has been damaged or destroyed over large areas
298 of the island and this likely increased the hydrological recharge. Therefore, a general increase in
299 recharge in the catchment area could be a contributing mechanism behind the long-term trend of
300 rising water levels in the Belham valley. To estimate this effect would require piezometric data
301 with the same hydrological regime as the Belham aquifer but not influenced by the volcano;
302 unfortunately these data do not exist. Due to the significant temporal and spatial variations and
303 unknowns regarding the hydrological dynamics of the system (e.g. the hydraulic properties of the
304 aquifer, its connectivity to recharge locations, as well as the exact catchment area, are unknown),
305 the explicit quantification of this contribution is beyond the scope of this paper and will be
306 addressed in a hydrologically focussed study at later stage.

307 Here, we explore scenarios related to volcanic activity causing the observed signals. The
308 most prominent long-term stress changes on Montserrat are due to the inflation-deflation cycles of
309 SHV, however, water levels increased during both repose and lava dome extrusion phases (Fig.
310 2a). Therefore, the overall trend of water level change is not related to reservoir pressure changes
311 and lava extrusion at SHV. A short-term signal in water levels could be linked to seismic stress.

However, the seismic record for the time period of the observed water level fall in May 2006 does not indicate either unusually low or high activity (e.g. Loughlin et al., 2006).

Instead, we propose lahar sedimentation and a dome collapse as driving forces behind poroelastic water level changes in the Belham valley.

4.1 Hypothesis 1: Lahar loading

The Belham valley was inundated by numerous lahars after the onset of the eruption, during both repose and extrusion phases (Froude, 2015; Alexander et al., 2010; Donnelly, 2015; Barclay et al., 2007). Ten and 23 lahars are confirmed or regarded as very likely to have entered the valley in 2005 and 2006, respectively (Froude, 2015). The lahars are caused almost exclusively by rainfall, which mobilises loose volcanic deposits in the upper catchment and transports material downstream towards the coast (Barclay et al., 2007). Lahar occurrence is therefore much higher in the rainy season compared to the dry season, with October showing the highest lahar incidence of 3.4 lahar days per month and February having the least lahars with 0.3 lahar days per month (averaged from the lahar record 1995-2013) (Froude, 2015). Since flow volume data are not available, Froude (2015) distinguished lahar sizes based on their duration and flow width: 6% of all lahars occupied most of the valley floor and lasted for over 24 hours, 29% occupied more than 50% of the valley floor and persisted for more than 12 hours, while 65% were confined to a single channel and lasted just a few hours. The lahar sediment deposition has led to an average sediment aggradation of 0.4 m per year, dramatic geomorphic changes - including a significant seaward movement of the shoreline - and deep burial of houses and infrastructure (Froude, 2015). An increase in the sediment burden affects underlying water-saturated porous media by increasing the pore pressure (e.g. Boutt, 2010). We therefore propose that the long-term water level increase in the Belham aquifer is caused by the increasing sediment load due to repeated lahars (*hypothesis*

1). Since the lahars are induced by rainfall, cumulative rainfall data are related to cumulative lahar loading, and the good correlation of cumulative rainfall data with well observations (Tab. 1) supports this hypothesis. The periodicity of water levels can therefore be linked to the higher number of lahars during the rainy season and the absence of rainfall-induced lahars during the dry season.

4.2 Hypothesis 2: Dome collapse

The timing of the single notable water level decrease (31st of May 2006) is significant, since a wholesale lava dome collapse occurred on 20 May 2006 (Fig. 2a), removing 97 Mm^3 of material from the summit (Ryan et al. 2010; Loughlin et al. 2010; Trofimovs et al. 2012). The dome material travelled down the volcano's eastern flank (i.e. away from the wells) and most was deposited offshore. We propose that the short-term water level decrease in the Belham aquifer is related to strain induced by the dome collapse. A direct poroelastic response, however, would be immediate. Additionally, due to the distance of the strain source, a direct elastic response in the shallow, unconsolidated Belham aquifer will be small or even negligible, because sufficient strain-coupling requires more competent lithologies at these distances. Therefore, we suggest that the collapse induced a significant hydraulic head drop in a second, deeper-seated aquifer (in line with suggestions by Hemmings et al. (2015a, 2015b)), which is more competent and connected to the Belham aquifer by vertical fractures. This would cause porous and/or fracture flow between the aquifers and thus explain the time delay between dome collapse and water level fall in the Belham aquifer. The Belham valley is a fault zone with a fracture network that can facilitate such connections (Hautmann et al., 2010; Feuillet et al., 2010; Kenedi et al., 2010). Furthermore, Bouguer anomalies suggest a significant shift in rock density in the Belham valley at depths greater than 600 m (Hautmann et al., 2013) and, while recent volcanic deposits from SHV are not usually

of a sufficient Young's Modulus (Young and Gottsmann, 2015), the compaction and hydrothermal consolidation by geothermal fluid input (proposed by Jones et al. (2010)) could increase the stiffness of a deeper-seated aquifer. The connection between the aquifers may be intermittent - fractures can form and widen (increasing permeability) due to seismic or other perturbances and become sealed again with time (e.g. Montgomery and Manga, 2003, Rojstaczer and Wolf, 1992, Elkhoury et al., 2006, Shi et al., 2015, Geballe et al., 2011).

Crustal strain due to dome collapse has two origins. The first is unloading of the summit surface due to the removal of weight. The second strain source is magma chamber inflation as a result of surface unloading. Recorded strain data associated with the dome collapse in July 2003 were interpreted by Voight et al. (2006) to indicate inflation of SHV's shallower magma chamber shortly after the collapse (see also Chen et al., 2018). Voight et al. (2006) propose that the drop in lithostatic load due to the collapse led to vesiculation of the resident magma, causing a rapid (about 4 h) build-up of pressure after the collapse. We suggest that similar processes were associated with the 2006 dome collapse and that the Belham aquifer system responded to these volcanic strains (i.e. unloading from the dome and short-term increase of chamber pressure) as a poroelastic medium, which in turn can explain the observed water level changes (*hypothesis 2*).

Both hypotheses are illustrated in a conceptual model in Fig. 3. In the following we test these hypotheses and explore the associated mechanisms by simulating the scenarios in numerical models that account for poroelastic deformation of the aquifer.

5 Methods

We apply poroelastic models developed by Strehlow et al. (2015) in the finite element analysis software COMSOL Multiphysics (version 5.1), benchmarked against a known analytical solution for a poroelastic problem (see online resource 2). While some problems presented in this study could be solved analytically, we implemented finite element models because they allow us to include stratigraphy and topography easily. These time-dependent, 2D-axisymmetric models solve fully-coupled solid mechanics and porous flow equations to simulate crustal deformation and the resulting pressure changes and fluid flow in a water-saturated, confined aquifer. Additional hydrological sources and sinks are neglected. The generic models are adapted to incorporate available information on aquifer properties, strain sources and surrounding lithologies on Montserrat. We assume linear elastic and poroelastic behaviour of the surrounding crust and the aquifer domain, respectively. The simulated flow is isothermal. Chosen material properties are based on literature (Freeze and Cherry, 1979, Fetter, 1994, Wang, 2000, Gercek, 2007, Gudmundsson, 2011, Adam and Otheim, 2013, geotechdata.info, 2013, Sevilla et al., 2010, Young and Gottsmann, 2015, Hemmings et al., 2015a). All reference values of input parameters are listed in Table 2; more details and ranges for parameter sweeps are provided in online resource 3. We run the simulations with both aquifer properties representing the Belham aquifer, and for a stiffer, less permeable aquifer (model acronyms with an "s"-subscript), representing lava or a more consolidated pyroclastic deposit.

The initial pore pressure in the aquifer is set as hydrostatic. The model solution gives solid displacement **u** and fluid pore pressure p_f. For comparison with the observed water table changes, we present model results as the hydraulic head: $h = \frac{p_f}{\rho_f \times g} - z$ (1) (ρ_f: water density, g:

gravitational acceleration, *z*: depth coordinate), which is proportional to pore pressure and represents the maximum water level change in a small diameter well in a confined aquifer. As the wells move with the ground, vertical ground displacement is subtracted from this hydraulic head change to obtain the relative water level change that would be measured in the wells.

5.1 Models

Our hypotheses involve a stacked, two-aquifer system in the Belham valley with a (possibly intermittent) connection through pores and/or fracture flow. Since the type and diffusivity of this connection is unknown, and in order to be able to independently resolve and understand hydrological processes in response to different strain sources in detail, we set up two suites of models. The first set of models simulates the effect of lahar loading on an aquifer ("lahar models", acronym L). The second set simulates aquifer response to strain due to a dome collapse ("collapse models", acronym COL). The more complex response of a stacked aquifer system significantly limits the efficiency of the models and is out of the scope of this study and left for future work. The presented models assume a confined, water-saturated aquifer that does not undergo significant temperature changes during the period of interest (for more details see Strehlow et al. (2015)). These are valid assumptions at least for the local vicinity of the wells, since temperatures have

been approximately constant in the past (Hemmings et al., 2015b) and the Belham aquifer was saturated during the whole period of observations.

5.1 Lahar models

To investigate the influence of sediment loading and test hypothesis 1 ("lahar models", acronym L), we define the system as shown in Fig. 4a consisting of a linear elastic solid block with an embedded shallow poroelastic aquifer that is water-saturated and confined. The duration of the time-dependent simulation is 3 years. We apply a time-dependent upper boundary load to the surface that corresponds to an annual sediment aggradation a (reference value of 0.4 m/a):

$$\Delta P_{lahar}(t) = \rho_{sediment} \times g \times a \times t \quad (2)$$

with $\rho_{sediment}$ the density of the deposited sediment and t time. In the first suite of models, we investigate a (temporally) linear loading. Since lahar frequency is coupled with rainfall (Barclay et al. 2007), we then adapt the load such that it mirrors the inter-seasonal variation in rainfall on Montserrat (model acronym Lc): no load is applied in the dry season (February to April), while the load during September to November is twice as high as in the remaining months, following the seasonality of rainfall outlined in Hemmings et al. (2015a). The reference lahar model with cyclic loading (L_c) can be found as an .mph file in online resource 4.

5.2 Collapse models

Fig. 4b shows the geometry used to test hypothesis 2 ("collapse models", acronym COL), which includes an approximation of the volcano's topography and its magmatic plumbing system (magma chambers are represented as cavities in the domain). The aquifer in these simulations does not cover the whole domain but starts at a variable lateral distance from the volcanic summit: as a

reference value, we chose the distance from the vent to the Belham valley fault. We simulate crustal deformation associated with dome collapse and growth, which resumed immediately afterwards, by assigning boundary loads that represent the two sources contributing to generated strain: the loading and unloading of the summit's surface by the weight of the dome material, and the inflation and deflation of the volcano's plumbing system. The duration of the time-dependent simulation is 200 days.

Loading of the summit: A total rock volume of V_{Dome}=97 Mm3 (dense rock equivalent) was removed from the summit during the May 2006 dome collapse (Loughlin et al. 2010). Assuming a cylindrical dome with a base radius r_{Dome} of 0.5 km, we can define the unloading function as:

$$\Delta P_{collapse} = -\rho_{lava} \times g \times h_{av} = -2600 \frac{kg}{m^3} \times g \times \frac{V_{Dome}}{\pi \times r_{Dome}^2} = -3.15\ MPa \quad (3)$$

with ρ_{Lava} the average density of extruded dome lava (2600 kg/m3) and h_{av} the average height of the dome at the time of collapse. Most of the dome collapse occurred in less than 1 hour (Loughlin et al., 2010), so we ramp up this collapse function linearly from 0 to 100% over the duration of 1 hour.

Using the average extrusion rate $\frac{V}{t}$ of the dome in the period after the dome collapse (which was roughly constant – see Fig. 2a), we can also define the time-dependent loading function for the summit during dome growth using the dome volumes in Loughlin et al. (2010):

$$\Delta P_{growth}(t) = \rho_{lava} \times g \times \frac{V}{t} \times \frac{1}{\pi \times r_{Dome}^2} \times t = 0.237\ \frac{Pa}{s} \times t \quad (4)$$

This function is set to start after one hour of the simulation has passed.

Loading of the magmatic plumbing system: Here, we assume the existence of two stacked magmatic chambers (following Hautmann et al. (2014)) with the lower magma chamber (LMC) at about 13 km depth and the upper magma chamber (UMC) at about 6 km depth (Fig. 4b).

The derived pressure build-up in the UMC due to vesicle formation and growth following the July 2003 collapse was about 4 MPa (Fig. 4 in Voight et al. (2006)). Unfortunately, no strain data exist for the May 2006 collapse. Because the removed dome volume during the 2006 collapse was about half that of the 2003 collapse (97 vs 200 Mm^3), we assume a pressure increase of $\Delta P_{UMC,col} = 2$ MPa during the 2006 collapse as a first order estimation. This is applied as a boundary load on the UMC, whereby the load is linearly ramped up over the duration of 1 hour.

For lack of better data, we apply the simplified equation

$$\Delta P = \frac{1}{\beta}\frac{\Delta V}{V} \quad (5)$$

for first-order estimation of depressurization values for the UMC and LMC during dome growth, using the volume changes derived by Mattioli et al. (2010) for SHV's third phase of dome extrusion. Gottsmann and Odbert (2014) infer a range of 1 to 10 GPa for the magma bulk modulus; we use $\frac{1}{\beta} = 7$ GPa following Linde et al. (2009). The derived boundary loads are $\Delta P_{UMC,grow} = -0.4$ MPa and $\Delta P_{LMC} = -17$ MPa. Due to the simplifications and the uncertainties in volume changes and the magma bulk modulus, there are large uncertainties associated with these depressurization values, but they suffice for a proof-of-concept model. To take the uncertainties into account, we vary depressurization values in parametric sweeps to test the sensitivity of the model to these values. The third phase of dome extrusion lasted for 627 days; assuming linear

deflation, we use the following time-dependent functions that are applied as a boundary load to UMC and LMC, respectively, once the simulation has run for 1 hour (i.e. after dome collapse is over):

$$\Delta P_{UMC,grow}(t) = \frac{\Delta P_{UMC,grow}}{627d} \times t \quad (6)$$

$$\Delta P_{LMC}(t) = \frac{\Delta P_{LMC}}{627d} \times t. \quad (7)$$

The reference collapse model (COL) can be found as an .mph file in online resource 5.

Extensive sensitivity studies on input parameters for both lahar and collapse models were performed. Since the wells are less than 2 km from the coastline, and a lateral connection of the aquifer to the open ocean is conceivable, we tested the effect of a constant water table at the lateral aquifer boundary in the lahar models by setting the lateral boundary condition of the aquifer to h = 0 m at all times. We also tested the effect of topography (as shown in Fig. 4b) and a topography-dependent sediment load on the aquifer pressures in the lahar models. To define the sediment load function, we used the difference in pre-eruptive and current valley floor elevation as presented in Froude (2015) (see online resource 6). The explored parameter space and results of these tests can be found in online resources 3, 7 and 8.

6 Lahar models: results and discussion

6.1 Results of the reference simulation

In the reference simulation of the Belham aquifer, for both the linear (L) and cyclic loading (Lc) models, the simulated hydraulic head rises by about 2 m during the 3 years of increasing

497 sediment load. The cyclic loading is closely mirrored in the aquifer pressure: the hydraulic head
498 rise is strongest during times of largest sediment load (the wet season) and constant during the dry
499 seasons, when no new load is applied (Fig. 5a).

500 For comparison, we also ran the models with a stiffer and less permeable aquifer (models
501 L_s and Lc_s). Under the same loading conditions, the hydraulic head in the stiffer aquifer rises by
502 only 0.2 m during 3 years of simulation duration. Thus, simulated head changes in the stiffer
503 aquifer are too small by an order of magnitude (Fig. 5a).

504 The main deviation between the reference model and observations in the Belham valley
505 occurs prior to the onset of dome growth (i.e. during the first 212 days). The observed water level
506 increases between January and March 2005, while the model predicts only a small increase in
507 January and a constant well level from February to April. Subsequently, observed well levels fall
508 between June and August 2005, when the model predicts increasing hydraulic heads. After
509 eruption onset, the simulated hydraulic head largely parallels that observed in the Belham aquifer.
510 Minor deviations after eruption onset can still be found during dry seasons, in which observed
511 hydraulic heads fall, while the simulated heads stay constant, and in the period following the dome
512 collapse, where the observed increase in hydraulic head is slightly stronger and less periodic than
513 predicted by our models.

514 6.2 Sensitivity analysis

515 To investigate the influence of input parameters, we performed parametric sweeps
516 regarding aquifer properties, the sediment load and boundary conditions. This section presents the

most important results of the sensitivity analysis, additional information can be found in Online Resource 7.

Amongst aquifer properties, the Young's Modulus is the most influential parameter. The softer the aquifer, the stronger is the hydraulic head response to the load at the surface (Fig. 5b-c). This matters most in stiffer aquifers: while a decrease of the Young's Modulus from 100 to 0.5 MPa has negligible influence, the decrease from 100 to 0.5 GPa increases the final hydraulic head rise from $h \approx 0.1$ to $h \approx 2$ m. Additional sensitivity studies regarding aquifer properties can be found in Online Resource 7.

We varied the applied sediment load by changing the assumed sediment thickness and density in the calculation for resulting load. Both parameters have a significant influence on the resulting aquifer pressure; the higher the sediment density and/or the sediment thickness, the stronger the hydraulic head rise (Fig. 5d-e). Within the tested range, a hydraulic head increase of up to $h \approx 8$ m in the soft, and $h \approx 0.8$ m in the stiff aquifer is reached after 3 years.

While the hydraulic head in the aquifer is spatially homogeneous in other simulations, it varies laterally in simulations with a constant water table at the lateral aquifer boundary (representing a connection to the ocean): the closer to the “ocean”, the smaller is the total head rise (Fig. 6a-b). This leads to hydraulic head decreases during phases with less or no sediment load due to pressure equilibration in the aquifer, which is facilitated by porous flow towards the boundary. A similar effect occurs in models that incorporate topography and a topography-dependent sediment load on the aquifer pressures: the hydraulic head at the well location decreases during dry seasons as opposed to staying constant in the reference simulation (Fig. 6c-d). This is again due to lateral

pressure variations in the aquifer - the hydraulic head is larger closer to the summit due to the higher sediment load - which induces porous flow away from the well location.

6.3 Discussion: long-term water level rise by sediment loading

Since rain is the main trigger for lahars on Montserrat, the good correlation of cumulative rainfall and water level increases supports the hypothesis of increased (cumulative) lahar deposit loading as a mechanism for the pressure increase in the Belham aquifer. The simulated hydraulic heads in the aquifer induced by sediment loading are of the right order of magnitude and show similar patterns to the observed water level rise. However, there are some clear deviations in the periodicity of the simulated and observed water levels before eruption onset where observed water levels rise during the dry period in early 2005. One possible explanation is that the seasonality of the water level signal prior to eruption onset is dominated by seasonal recharge. The recharge signal in water levels is likely to lag behind the precipitation seasons, thus explaining a rise in water levels with some delay after the wet season. After eruption onset, more loose sediment is available and more lahars enter the valley, thus the seasonal signal now becomes dominated by rainfall seasons. Since our models do not account for recharge, this effect cannot be resolved with this study.

In the months directly following the dome collapse in May 2006, the observed increase in water levels is slightly stronger than predicted by our models and lacks the clear seasonality prior to this event. This might be due to the significant shift in sediment deposition after the collapse, which led to heavily loaded lahars even during seasons with usually few or no lahars. This effect was also not included in our models.

Several parameters influence how the aquifer responds to the surface loading, but aquifer stiffness and sediment load are the most influential, indicating that the hypothesized deeper and

stiffer aquifer is unlikely to contribute significantly to the water level signal due to lahar sedimentation. Boundary conditions come into play in periods representing the dry season, when observed water levels decrease slightly, which according to our models can be explained with a link of the aquifer to the ocean and/or topography-dependent loading. There is definitely some topography-dependent loading as sedimentation in the Belham valley is not spatially homogeneous. This causes pressure imbalances and thereby porous flow in the aquifer from higher to lower pressures, leading to the observed water level decreases in dry seasons.

We cannot exclude the possibility of additional factors driving the water level rise in the Belham valley. In particular, as outlined in section 4, an increase in recharge can be a significant driver of rising water levels. Our models do show, however, that the effect of lahar loading is significant, consistent with the observations and causes a non-negligible effect on pore pressures in the aquifer. The detailed sensitivity studies (see also online resource 7) show that this holds true for a wide range of aquifer properties and boundary conditions. Hence, in the analysis of well water levels, the poroelastic effect caused by increasing sediment load must not be disregarded. The periodicity of the signal may be explained with the seasonality of rainfall and thus lahars. But this seasonality can also be seen in hydrological recharge and atmospheric pressure and, as discussed above, there are indications for a seasonal recharge signal in the water level data prior to eruption onset. Since precipitation, atmospheric pressure, lahars and recharge are all inherently coupled, it is not possible to distinguish individual signals with the available data.

7 Collapse models: results and discussion

7.1 Results of the reference simulation

With parameters at reference values, the temporal evolution of hydraulic head in the stiffer aquifer (COL_s) follows loading due to dome collapse and growth closely: the hydraulic head falls during the collapse to $h \approx -14$ cm and then immediately starts to rise again during renewed dome growth reaching about $h \approx 17$ cm at 200 days (Fig. 7a). The modelled water level fall during dome collapse in the stiff aquifer (COL_s) is similar to the observed value, but occurs simultaneously with dome collapse, while the observed drop has a time delay of 6-11 days after the collapse (there are no data points available between the 25th and 31st of May). The response of the stiff aquifer to dome growth-related strain is smaller than observed water level increases by a factor of 4.

The hydraulic head in the simulated less competent Belham aquifer (COL) falls by about 0.05 cm during dome collapse. It then continues to fall until about 20 days after the collapse to reach a minimum of $h \approx -0.15$ cm, which is two orders of magnitude less than the observed values.

Loading due to dome growth then leads to a head rise, reaching $h \approx 0.1$ cm at the end of the simulation, i.e. at 200 days (Fig. 7a).

7.2 Sensitivity analysis

To investigate the influence of input parameters, we performed parametric sweeps regarding aquifer properties and magma chamber loads. Here, we show only the most important results, additional sensitivity studies can be found in Online Resource 8.

Results of parametric sweeps on the aquifer's Young's Modulus (Fig. 7b-c) indicate that the difference in stiffness between the two types of aquifers is the main cause for the differing hydraulic head changes in response to dome collapse. Generally, the larger the Young's Modulus, the larger are the decreases in hydraulic head following dome collapse and the increases in hydraulic head during dome growth. Increasing the Young's Modulus of the soft aquifer to 100 MPa increases the head fall to $h \approx -1$ cm; the largest head fall is reached for E=50 GPa with $h \approx -14$ cm. Additionally, the time between dome growth onset and onset of hydraulic head rise is shorter the larger the Young's Modulus.

Aquifer depth also significantly affects the resulting hydraulic head fall in the COL model suite. At a depth of 1.5 km, the simulated collapse-related fall in hydraulic head in the Belham aquifer is $h \approx -11$ cm (Fig. 7d). In the stiffer aquifer, hydraulic head fall is smallest for an aquifer depth of 1 km, and is larger for shallower or deeper aquifers (Fig. 7e). However, the influence of aquifer depth on changes in hydraulic head in the stiff aquifer is small in comparison with other parameters.

7.3 Discussion: short-term water level fall by dome collapse-related strain

As expected (see section 4), simulated strains related to dome growth and collapse cause a very small response in the reference Belham aquifer. Simulated hydraulic heads fall to their minimum values with a time delay of several days after the dome collapse, but the fall is two orders of magnitude smaller than observed. Many parameters influence this result (see also online resource 8). However, the only model which produces the observed magnitude of hydraulic head decrease in a soft aquifer invokes a 1.5 km deep aquifer (Fig. 7d). The observation wells tap a soft, shallow aquifer, which therefore, according to our models, would not respond to dome-collapse related strains.

Since it responds to sediment load, the Belham aquifer would also respond to erosion, i.e. the removal of sediment burden. The long-term trend in the valley is sediment aggradation but during individual events or episodes, local erosion commonly occurred in the form of channel incision (Alexander et al., 2010, Froude, 2015). We therefore tested whether this could be an alternative explanation for the water level fall after the May 2006 dome collapse, which was followed by a period of intense lahars. But the simulated channel incision only causes a sufficiently large hydraulic head drop if there is large scale (at least 50 cm deep), almost valley-wide (50-100 m wide) erosion (see online resource 9), which did not occur.

However, dome collapse-related strain produces the right order of magnitude of hydraulic head fall in a much stiffer and less permeable aquifer. As expected for a poroelastic medium, the simulated response is instantaneous, while the observed response is delayed by at least 6 days. The hydraulic heads in this aquifer increase in response to dome growth, to about 25% of observed values.

Model results for a stiff aquifer hence support the hypotheses that the shallow Belham aquifer is connected to a second, stiffer aquifer and that the significant pressure drop due to dome-

collapse in that stiffer aquifer leads to water leakage from the Belham aquifer. This would then cause well levels in the Belham aquifer to drop with some delay. Hemmings et al. (2015a, 2015b) have already proposed the existence of a deeper aquifer in the Belham valley. As discussed in section 4, an increase in rock density and competence at greater depths is reasonable and it is likely that the deeper-seated aquifer is connected with the Belham aquifer by vertical fractures. The connection between the aquifers may be intermittent or permanent. If the Belham aquifer is fully connected to a stiffer aquifer at all times, the pressure increase in the stiffer aquifer due to dome growth could be contributing to the observed hydraulic head rise. The well level rise can be explained solely with lahar loading, but parameter uncertainties in our models are such that we cannot discard processes with certainty.

For a first-order investigation, we ran an additional simple 2D simulation, incorporating two stacked aquifers that are separated by an aquitard, but connected by vertical fractures (see online resource 10). Initialising the deeper aquifer at a hydraulic head of -0.1m indeed leads to downward fluid flow through the fractures and a hydraulic head fall in the upper aquifer reaching -0.09 m after 11 days with the chosen parameters. This further confirms the feasibility of our hypothesis, although the uncertainties regarding geometry and material properties are significant. More sophisticated modelling and detailed parameter studies of such a two-aquifer model, in particular one that also incorporates the lahar loading, is beyond the scope of this study and left for future work.

No strain data exist for the time period considered here. Data series from the GPS network show no clear indication for ground deformation at proximal sites and no evidence for any deformation in the Belham Valley associated with the dome collapse in May 2006 (Pascal et al., 2017). Under the assumption that the well level changes are indeed caused by dome collapse-

related strain, we can utilise these to draw implications about crustal strain. We applied two strain sources during dome collapse in our simulations: pressure build-up of the UMC and unloading of the summit. Both sources can cause a hydraulic head fall of similar magnitude and most likely acted together (see online resource 11). Therefore, the water level record indicates a pressure build-up in the upper magma chamber during a dome collapse, supporting the conclusions drawn from strainmeter data in 2003 by Voight et al. (2006).

8 Conclusions

Volcanic strain has been the suggested driver behind water level changes at many volcanoes, but this process has so far not been sufficiently quantitatively tested. Strehlow et al. (2015) developed numerical models to investigate a hypothetical scenario of poroelastic aquifer responses to magma chamber inflation. This study has now extended these efforts by adapting the models to a real field scenario with specific water level observations, illustrating that poroelastic effects are not purely theoretical but can play an important role in real monitoring data.

Even though the results do not perfectly match the observations, the presented simulations can help to decipher origins of observed water level changes in the Belham valley on Montserrat, that comprise both a long-term well level rise over the period 2004-2006 and a short-term water level fall in May 2006. Simulated pore pressures in the Belham aquifer increase significantly due to the long-term sediment deposition by repeated lahars in the valley, which in turn leads to a well water level rise. While not notably affecting the Belham aquifer itself, simulated crustal strains associated with the dome collapse in May 2006 lead to a significant water level drop in a more competent aquifer. Thus, water could leak from the Belham aquifer e.g. through connecting

683 fractures, into a deeper-seated, stiff aquifer, thereby causing a noticeable well level drop days after
684 the collapse.

685 Therefore, the suggested conceptual model shown in Fig.3 represents one possible
686 explanation for the water level observations between 2004 and 2006: We suggest that both
687 sediment accumulation and dome collapse significantly affected the hydraulic head in the Belham
688 aquifer on different timescales. While additional hydrological drivers cannot be excluded with
689 absolute certainty, the suggested processes can serve as a possible explanation for the observed
690 water level variations and cannot be neglected in the analysis of well water levels.

691 Our study shows that groundwater dynamics in relation to volcanic activity as predicted
692 from theoretical modelling (Strehlow et al. 2015) can indeed be witnessed in field observation data
693 and that volcanic strain from various sources strongly affects water levels in regional aquifers on
694 different time scales. Therefore, this study represents an intermediate step between the theoretical
695 analysis in Strehlow et al. (2015) and the incorporation of water level observations in volcano
696 monitoring systems. The inferred underlying processes are not unique to the island of Montserrat
697 and as such make our results transferable to other volcanic and hydrological settings, where the
698 observation and interpretation of water levels can also provide important insights regarding the
699 state of volcanoes.

700

701 8.1 Future work

702 While our study provides a possible first-order explanation for observed water level
703 variations in the Belham valley, there are still deviations between the model results and
704 observations and our models include several simplifications and unknowns. To fully exploit the
705 potential of water level observations within volcano monitoring systems, both further development

of the numerical models and more sophisticated hydrological data acquisition and analysis are necessary. We recommend:

- A quantification of seasonal and long-term variations in hydrological recharge, and incorporation into the models.
- The development of full three-dimensional models to truly incorporate topographic and stratigraphic features of Montserrat both on-land and offshore.
- The development of a stacked two-aquifer model that combines the effects of strain due to lahar loading and dome collapse in one simulation.
- The set-up of inversion models to acquire a best-fit model to the observations.
- (For any volcano:) The routine acquisition of high-quality, high-resolution water level data, in order to resolve barometric and tidal effects on the aquifer. Since tidal strains are known, the response to tides can then be used to calibrate water wells as strainmeters and help to ground-truth numerical models (e.g. Roeloffs 1996; Wang 2000).

References

Availability of data and models: All data used in this study, as well as reference models (.mph files to be opened in COMSOL Multiphysics) for both the lahar and the collapse models can be found in the supplementary materials online (online resources 4, 5 and 12).

Adam L and Otheim T (2013) Elastic Laboratory Measurements and Modeling of Saturated Basalts. J Geophys Res - Sol Ea, 118:840–851.

727 Alexander J, Barclay J, Sušnik J, Loughlin S, Herd R, Darnell A, Crosweller S (2010) Sediment-
728 charged flash floods on Montserrat: The influence of synchronous tephra fall and varying
729 extent of vegetation damage. J Volcanol Geoth Res, 194:127–138.
730 Barclay J, Alexander J, Sušnik J (2007) Rainfall-induced lahars in the Belham Valley, Montserrat,
731 West Indies. Journal of the Geological Society, London, 164:815–827.
732 Brodsky E, Roeloffs E, Woodcock D, Gall I, and Manga M. (2003). A mechanism for sustained
733 groundwater pressure changes induced by distant earthquakes. J Geophys Res - Sol Ea,
734 108(B8).
735 Capasso G, Federico C, Madonia P, and Paonita A (2014). Response of the shallow aquifer of
736 the volcano-hydrothermal system during the recent crises at Vulcano Island (Aeolian
737 Archipelago, Italy). J Volcanol Geoth Res, 273:70–80.
738 Chen C-W, Huang H-F, Hautmann S, Sacks IS, Linde AT, Taira T (2018) Resonance oscillations
739 of the Soufrière Hills Volcano (Montserrat, W.I.) magmatic system induced by forced
740 magma flow from the reservoir into the upper plumbing dike. J Volcanol Geoth Res, 350:7-
741 17.
742 Coco A, Gottsmann J, Whitaker F, Rust A, Currenti G, Jasim A, and Bunney S (2016).
743 Numerical models for ground deformation and gravity changes during volcanic unrest:
744 simulating the hydrothermal system dynamics of a restless caldera. Solid Earth, 7:557–
745 577.
746 Costa A, Melnik O, Sparks RSJ, and Voight B (2007) Control of magma flow in dykes on cyclic
747 lava dome extrusion, Geophys Res Lett, 34, L02303, doi:10.1029/2006GL027466.
748 Boutt D (2010) Poroelastic Loading of an Aquifer Due to Upstream Dam Releases. Groundwater,
749 48(4):580–592.

750 Donnelly L (2015) Engineering geology of landslides on the volcanic island of Montserrat, West
751 Indies. Quarterly Journal of Engineering Geology and Hydrogeology, 40:267–292.
752 Dundas C and Keszthelyi L (2013) Modeling steam pressure under Martian lava flows. Icarus,
753 226(1):1058–1067.
754 Elkhoury J, Brodsky E, Agnew D (2006) Seismic waves increase permeability. Nature,
755 441(7097):1135–1138.
756 Fetter C (1994) Applied Hydrogeology. Macmillan Company, New York
757 Feuillet N, Leclerc F, Tapponnier P, Beauducel F, Boudon G, Le Friant A, Deplus C, Lebrun J-F,
758 Nercessian A, Saurel J-M, Clément V (2010) Active faulting induced by slip partitioning
759 in Montserrat and link with volcanic activity: New insights from the 2009 GWADASEIS
760 marine cruise data. Geophys Res Lett, 37(19).
761 Fournier N and Chardot L (2012). Understanding volcano hydrothermal unrest from geodetic
762 observations: Insights from numerical modeling and application to White Island Volcano,
763 New Zealand. J Geophys Res - Sol Ea, 117(B11):doi: 10.1029/2012JB009469.
764 Freeze R and Cherry J (1979) Groundwater. Prentice-Hall, Englewood Cliffs, N.J.
765 Froude M (2015) Lahar dynamics in the Belham River Valley, Montserrat: Application of remote
766 camera-based monitoring for improved sedimentological interpretation of post-event
767 deposits. PhD thesis, School of Environmental Sciences, University of East Anglia,
768 Norwich.
769 Geballe Z, Wang C-Y, Manga M (2011) A permeability-change model for water-level changes
770 triggered by teleseismic waves. Geofluids, 11(3):302–308.
771 Geotechdata.info (2013) Soil Young's Modulus. http://geotechdata.info/parameter/soil-elastic-
772 young-modulus.html.

773 Gercek H (2007) Poisson's ratio values for rocks. Int J Rock Mech Min, 44(1):1–13.
774 Gottsmann J, De Angelis S, Fournier N, Van Camp M, Sacks S, Linde A, and Ripepe M (2011)
775 On the geophysical fingerprint of Vulcanian explosions. Earth Planet Sc Lett, 306(1-2):98–
776 104.
777 Gottsmann J and Odbert H (2014) The effects of thermomechanical heterogeneities in island arc
778 crust on time-dependent preeruptive stresses and the failure of an andesitic reservoir. J
779 Geophys Res - Sol Ea, 119(6):4926–4639.
780 Gudmundsson A (2011) Rock fractures in geological processes. Cambridge University Press.
781 Harford CL, Pringle MS, Sparks RSJ, and Young SR (2002) The volcanic evolution of Montserrat
782 using $^{40}Ar/^{39}Ar$ geochronology. In: The Eruption of Soufrière Hills Volcano, Montserrat
783 from 1995 to 1999, Geol. Soc. Mem., vol. Xx, edited by T.H. Druitt and B.P. Kokelaar,
784 doi: https://doi.org/10.1144/GSL.MEM.2002.021.01.05
785 Hautmann S, Gottsmann J, Sparks RSJ, Costa A, Melnik O, and Voight B (2009) Modelling
786 ground deformation caused by oscillating overpressure in a dyke conduit at Soufrière
787 Hills Volcano, Montserrat. Tectonophysics, 471, 87–95, doi:10.1016/j.tecto.2008.10.021
788 Hautmann S, Gottsmann J, Camacho AG, Fournier N, Sacks IS, Sparks RSJ (2010) Mass
789 variations in response to magmatic stress changes at Soufrière Hills Volcano, Montserrat
790 (WI): Insights from 4-D gravity data. Earth Planet Sc Lett, 290(1):83–89.
791 Hautmann S, Camacho AG, Gottsmann J, Odbert HM, Syers RT (2013) The shallow structure
792 beneath Montserrat (West Indies) from new Bouguer gravity data. Geophys. Res.
793 Lett., 40, 5113–5118, doi:10.1002/grl.51003.

794 Hautmann S, Witham F, Christopher T, Cole P, Linde A, Sacks IS, Sparks RSJ (2014) Strain field
795 analysis on Montserrat (W.I.) as tool for assessing permeable flow paths in the magmatic
796 system of Soufrière Hills Volcano. Geochem Geophys Geosyst, 15:676–690.
797 Hemmings B, Whitaker F, Gottsmann J, Hughes A (2015a) Hydrogeology of Montserrat review
798 and new insights. Journal of Hydrology: Regional Studies, 3:1–30.
799 Hemmings B, Gooddy D, Whitaker F, Darling W, Jasim A, Gottsmann J (2015b) Groundwater
800 recharge and flow on Montserrat, West Indies: Insights from groundwater dating. Journal
801 of Hydrology: Regional Studies, 4:611–622.
802 Hemmings B, Whitaker F, Gottsmann J (2012) Initial investigations of the productive perched
803 aquifers on the volcanic island of Montserrat. In Proceedings of the TOUGH Symposium
804 2012. Lawrence Berkeley National Laboratory, Berkeley.
805 Hurwitz S and Johnston MJ (2003). Groundwater level changes in a deep well in response to a
806 magma intrusion event on Kilauea Volcano, Hawai'i. Geophys Res Lett, 30(22):2173.
807 HydroSource (2004) Groundwater Exploration and Development of High Yield Water Supply
808 Wells for The Montserrat Water Authority. Technical Report. HydroSource Assoc. Inc.,
809 Ashland, New Hampshire.
810 Jasim A, Hemmings B, Mayer K, Scheu B (2018) Groundwater flow and volcanic unrest. In:
811 Gottsmann J, Neuberg J, Scheu B (eds.) Volcanic Unrest. Advances in Volcanology.
812 Springer, Cham. doi: 10.1007/11157_2018_33
813 Jones M, Hembury D, Palmer M, Tonge B, Darling W, Loughlin S (2011) The weathering and
814 element fluxes from active volcanoes to the oceans: a Montserrat case study. Bull Volcanol,
815 73(3):207–222.

816 Kenedi C, Sparks R, Malin P, Voight B, Dean S, Minshull T, Paulatto M, Peirce C, Shalev E
817 (2010) Contrasts in morphology and deformation offshore Montserrat: New insights from
818 the SEA-CALIPSO marine cruise data. Geophys Res Lett, 37(19).
819 Kokelaar BP (2002), Setting, chronology and consequences of the eruption of Soufrière Hills
820 Volcano, Montserrat (1995–1999). In: The Eruption of Soufrière Hills Volcano, Montserrat
821 from 1995 to 1999, Geol. Soc. Mem., vol. Xx, edited by T.H. Druitt and B.P. Kokelaar,
822 doi: https://doi.org/10.1144/GSL.MEM.2002.021.01.02
823 Kopylova GN and Boldina SV (2012). On the relationships of water-level variations in the E-1
824 well, Kamchatka to the 2008–2009 resumption of activity on Koryakskii volcano and to
825 large ($M \geq 5$) earthquakes. Journal of Volcanology and Seismology, 6(5):316–328.
826 Linde AT, Sacks S, Hidayat D, Voight B (2009) The Montserrat Soufrière Hills Explosion of
827 March 2004: Magma Geometry and Incompressibility from Borehole Strain Data., Eos
828 Trans. AGU, 89(53), Fall Meet. Suppl., Abstract V53C-02.

829 Linde AT, Sacks S, Hidayat D, Voight B, Clarke A, Elsworth D, Mattioli G, Malin P, Shalev E,
830 Sparks S, Widiwijayanti C (2010) Vulcanian explosion at Soufrière Hills Volcano,
831 Montserrat on March 2004 as revealed by strain data. Geophys Res Lett, 37, L00E07. doi:
832 10.1029/2009GL041988.
833 Loughlin S, Baptie B, Christopher T, Ryan G, Luckett R, Hards H, Jones L, Fournier N, Bass V,
834 Syers T, Ruzie L, Higgins M, Williams P, and Williams D (2006) Assessment of the
835 hazards and risks associated with the Soufriere Hills Volcano, Montserrat. Seventh Report
836 of the Scientific Advisory Committee on Montserrat Volcanic Activity, 28-30 August
837 2006: Part II, Technical Report, issued 23 September 2006.

838 Loughlin S, Luckett R, Ryan G, Christopher T, Hards V, De Angelis S, Jones L, Strutt M (2010)
839 An overview of lava dome evolution, dome collapse and cyclicity at Soufrière Hills
840 Volcano, Montserrat, 2005-2007. Geophys Res Lett, 37(L00E16).
841 Matsumoto N, Sato T, Matsushima N, Akita F, Shibata T, and Suzuki A (2002). Hydrological
842 anomalies associated with crustal deformation before the 2000 eruption of Usu volcano,
843 Japan. Geophys Res Lett, 29(5,1057), doi:10.1029/2001GL013968.
844 Mattioli G, Dixon TH, Farina FF, Howell ES, Jansma PE, and Smith AL (1998) GPS measurement
845 of surface deformation around Soufrière Hills Volcano, Montserrat, from October 1995 to
846 July 1996, Geophys Res Lett, 25, 3417–3420, doi:10.1029/98GL00931.
847 Mattioli GS, Herd R, Strutt M, Ryan G, Widiwijayanti C, Voight B (2010) Long term surface
848 deformation of Soufrière Hills Volcano, Montserrat from GPS geodesy: Inferences from
849 simple elastic inverse models. Geophys Res Lett, 37(L00E13).
850 Melnik O, and Costa A (2014) Dual chamber-conduit models of non-linear dynamics behaviour at
851 Soufrière Hills Volcano, Montserrat. In: The Eruption of Soufrière Hills Volcano,
852 Montserrat, From 2000 to 2010, Geol. Soc. Mem., vol. 39, edited by G. Wadge, R.,
853 Robertson, and B. Voight, 61–69, doi:10.1144/M39.3, Geol. Soc., London
854 Montgomery D and Manga M (2003) Streamflow and water well responses to earthquakes.
855 Science, 300(5628):2047–2049.
856 Newhall C, Albano S Matsumoto N, Sandoval T (2001) Roles of groundwater in volcanic unrest.
857 Journal of the Geological Society of the Philippines, 56:69–84.
858 Odbert HM, Stewart RC, and Wadge G (2014a) Cyclic phenomena at the Soufrière Hills Volcano,
859 Montserrat. In: The Eruption of Soufrière Hills Volcano, Montserrat from 2000 to 2010,
860 Geol. Soc. Mem., vol. 39, edited by G. Wadge, R., Robertson, and B. Voight.

Odbert H, Ryan G, Mattioli GS, Hautmann S, Gottsmann J, Fournier N, Herd R (2014b) Volcano geodesy at the Soufrière Hills Volcano, Montserrat: a review. In: The Eruption of Soufrière Hills Volcano, Montserrat from 2000 to 2010, Geol. Soc. Mem., vol. 39, edited by G. Wadge, R., Robertson, and B. Voight.

Pascal K, MVO Staff and Colleagues (2017) 22 years of volcano-deformation monitoring at Soufrière Hills Volcano, Montserrat. International Association of Volcanology and Chemistry of the Earth's Interior (IAVCEI) conference, Portland, USA. (Poster)

Paulatto M, Annen C, Henstock TJ, Kiddle E, Minshull TA, Sparks RSJ, and Voight B (2012) Magma chamber properties from integrated seismic tomography and thermal modeling at Montserrat. Geochem Geophys Geosyst, 13, Q01014, doi:10.1029/2011GC003892t

Rasmussen T and Crawford L (1997) Identifying and removing barometric pressure effects in confined and unconfined aquifers. Groundwater, 35(3):502–511.

Rice JR and Cleary MP (1976). Some Basic Stress Diffusion Solutions for Fluid-Saturated Elastic Porous Media With Compressible Constituents. Reviews of Geophysics and Space Physics, 14(2):227–241.

Roeloffs E (1996) Poroelastic techniques in the study of earthquake-related hydrologic phenomena. Adv Geophys, 37:135-195.

Rojstaczer S and Agnew D (1989) The influence of formation material properties on the response of water levels in wells to earth tides and atmospheric loading. J Geophys Res - Sol Ea, 94(B9):12403–12411.

Rojstaczer S and Wolf S (1992) Permeability changes associated with large earthquakes: An example from Loma Prieta, California. Geology, 20(3):211–214.

883 Rouwet D, Sandri L, Marzocchi W, Gottsmann J, Selva J, Tonini R, and Papale P (2014).
884 Recognizing and tracking volcanic hazards related to non-magmatic unrest: a review.
885 Journal of Applied Volcanology, 3(17):doi:10.1186/s13617–014–0017–3.
886 Ryan G, Loughlin S, James M, Jones L, Calder E, Christopher T, Strutt M, Wadge G (2010)
887 Growth of the lava dome and extrusion rates at Soufrière Hills Volcano, Montserrat, West
888 Indies: 2005-2008. Geophys Res Lett, 37(L00E08).
889 Sevilla W, Ammon C, Voight B, De Angelis S (2010) Crustal structure beneath the Montserrat
890 region of the Lesser Antilles island arc. Geochem Geophys Geosyst, 11(6).
891 Shalev E, Kenedi CL, Malin P, Voight V, Miller V, Hidayat D, Sparks RSJ, Minshull T, Paulatto
892 M, Brown L, Mattioli G (2010) Three-dimensional seismic velocity tomography of
893 Montserrat from the SEA-CALIPSO offshore/onshore experiment. Geophys Res Lett, 37,
894 L00E17, doi:10.1029/2010GL042498
895 Shi Z, Wang G, Manga M, Wang C-Y (2015) Mechanism of co-seismic water level change
896 following four great earthquakes–insights from co-seismic responses throughout the
897 Chinese mainland. Earth Planet Sc Lett, 430:66–74.
898 Shibata T, Matsumoto N, Akita F, Okazaki N, Takahashi H, and Ikeda R (2010a). Linear
899 poroelasticity of groundwater levels from observational records at wells in Hokkaido,
900 Japan. Tectonophysics, 483(3):305–309.
901 Stefansson V (1981). The Krafla geothermal field, in: Geothermal Systems: Principles and Case
902 Histories, pages 273–294. Wiley, New York.
903 Strehlow K, Gottsmann J, Rust A (2015) Poroelastic responses of confined aquifers to subsurface
904 strain and their use for volcano monitoring. Solid Earth, 6:1207–1229.

905 Takahashi H, Shibata T, Yamaguchi T, Ikeda R, Okazaki N, and Akita F (2012). Volcanic strain
906 change prior to an earthquake swarm observed by groundwater level sensors in Meakan-
907 dake, Hokkaido, Japan. J Volcanol Geoth Res, 215:1–7.
908 Todesco M, Rutqvist J, Chiodini G, Pruess K, and Oldenburg CM (2004). Modelling of recent
909 volcanic episodes at Phlegrean Fields (Italy): Geochemical variations and ground
910 deformation. Geothermics, 33:531–547.
911 Trofimovs J, Foster C, Sparks R, Loughlin S, Le Friant A, Deplus C, Porritt L, Christopher T,
912 Luckett R, Talling P, Palmer M, Le Bas T (2012) Submarine pyroclastic deposits formed
913 during the 20th May 2006 dome collapse of the Souffrière Hills Volcano, Montserrat. Bull
914 Volcanol, 74:391–405.
915 Voight B, Linde AT, Sacks IS, Mattioli GS, Sparks RSJ, Elsworth D, Hidayat D, Malin PE, Shalev
916 E, Widiwijayanti C, Young S, Bass V, Clarke A, Dunkley P, Johnston W, McWorther N,
917 Neuberg J, Williams P (2006) Unprecedented pressure increase in deep magma reservoir
918 triggered by lava-dome collapse. Geophys Res Lett, 33(L03312).
919 Wadge G, Robertson R, Voight B (editors) (2014) The Eruption of Soufrière Hills Volcano,
920 Montserrat from 2000 to 2010, Geol. Soc. Mem., vol. 39, edited by G. Wadge, R.,
921 Robertson, and B. Voight.
922 Wang, H. F. (2000). Theory of Poroelasticity with Applications to Geomechanics and
923 Hydrogeology. Princeton University Press.
924 Yokoyama I and Seino M (2000). Geophysical comparison of the three eruptions in the 20th
925 century of Usu volcano, Japan. Earth Planets and Space, 52(2):73–90.
926 Young N and Gottsmann J (2015). Shallow crustal mechanics from volumetric strain data: Insights
927 from Soufrière Hills Volcano, Montserrat. J Geophys Res - Sol Ea, 120:1559–1571.
928

Tables

Table 1: Correlation coefficients of different data sets with water levels in the Belham valley wells. Size of the water level data set is n=92

Data set	Correlation coefficient	p-Value	Size of dataset
Precipitation (daily)	-0.02	0.57	791
Precipitation (cumulative)	0.96	$< 10^{-9}$	791
Mean sea level pressure (daily)	0.13	$4x10^{-4}$	784
Mean sea level pressure(daily) – pre-collapse	0.28	$< 10^{-4}$	563
Mean sea level pressure (daily) – post-collapse	-0.33	$< 10^{-4}$	221
Mean sea level pressure (monthly)	-0.26	0.21	26
Mean sea level pressure (monthly) – pre-collapse	0.9	$< 10^{-4}$	19
Mean sea level pressure (monthly) – post-collapse	0.25	0.54	7

939 **Table 2**: Reference values of input parameters. Abbreviations: B-aq = Belham aquifer, S-aq = Stiff
940 aquifer, BW-coeff. = Biot-Willis-coefficient, Young's = Young's Modulus, Cap = the impermeable layer
941 above the aquifer

Parameter	Symbol & reference value	Parameter	Symbol & reference value
B-aq BW-coeff.	$\alpha = 0.7$	S-aq BW-coeff.	$\alpha = 0.3$
B-aq permeability	$\kappa = 1 \times 10^{-10}$ m2	S-aq permeability	$\kappa = 1 \times 10^{-14}$ m2
B-aq porosity	$\phi = 0.35$	S-aq porosity	$\phi = 0.1$
B-aq Young's	$E_{aq} = 10$ MPa	S-aq Young's	$E_{aq} = 50$ GPa
B-aq density	$\rho_{aq} = 2000$ kg/m3	S-aq density	$\rho_{aq} = 2800$ kg/m3
Aquifer thickness, L	$d_{aq} = 50$ m	Lateral distance	$L = 3$ km
Aquifer thickness, COL	$d_{aq} = 200$ m	Aquifer depth	$z_{aq} = 50$ m
Crust density	depth-dependent[a]	Water compressibility	$\chi = 4 \times 10^{-10}$ Pa-1
Crust Young's	depth-dependent[b]	Water density	$\rho_f = 1000$ kg/m3
Cap density	$\rho_{cap} = 2000$ kg/m3	Water viscosity	$\mu = 10^{-3}$ Pas
Cap Young's	$E_{cap} = 10$ MPa	Sediment aggradation	$a = 0.4$ m/a
Poisson's ratio	$\upsilon = 0.3$	Magma bulk modulus	$\frac{1}{\beta} = 7$ GPa
UMC centre depth	$z_{UMC} = 6$ km	LMC centre depth	$z_{LMC} = 12.5$km
UMC depressurization	$\Delta P_{UMC,grow} = -0.4$ MPa	LMC depressurization	$\Delta P_{LMC} = -17$ MPa
UMC radius	$r_{UMC} = 1.25$ km	LMC vertical semi-axis	$b_{LMC} = 2$ km
UMC pressure increase[c]	$\Delta P_{UMC,col} = 2$ MPa	LMC horizontal semi-axis	$c_{LMC} = 1.7$ km
Sediment density	$\rho_s = 1800$ kg/m3		

942 [a]Because the crust gets denser with depth, we use $\rho_c = 2800$ kg/m3 for depths <2 km and a ρ_c–vs-depth

943 function for greater depths as defined in Gottsmann and Odbert [2014] and Young and Gottsmann [2015].

944 [b]Because the crust gets stiffer with depth, we use $E_c = 5$ GPa for depths <2 km and a *E*-vs-depth function

945 for greater depths as defined in Gottsmann and Odbert [2014] and Young and Gottsmann [2015].

946 [c]during dome collapse

947

948

949

950

951

952

953

954

955

956

957

958

Figures

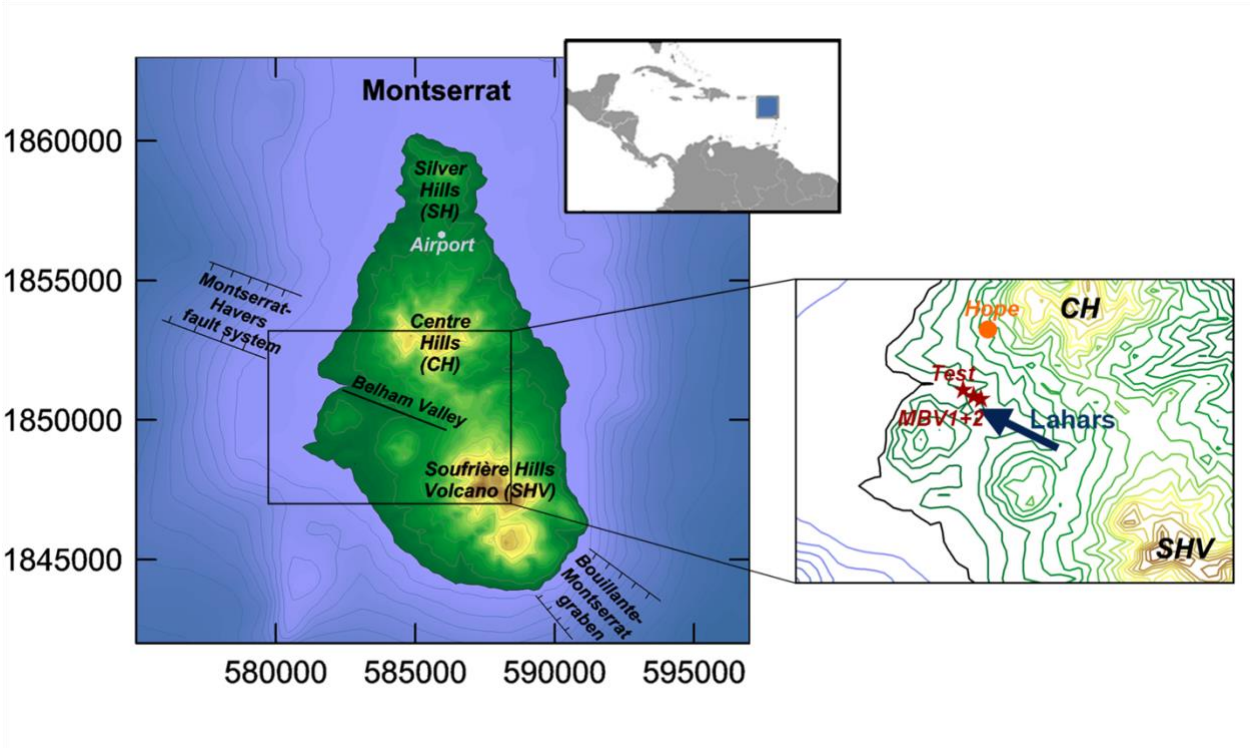

Fig. 1: Overview map of Montserrat and a zoom in on the Belham valley, with indicated well locations (MBV1, MBV2 and Test), the three volcanic centres, lahar flow directions, Montserrat's airport and the Hope rain gauge.

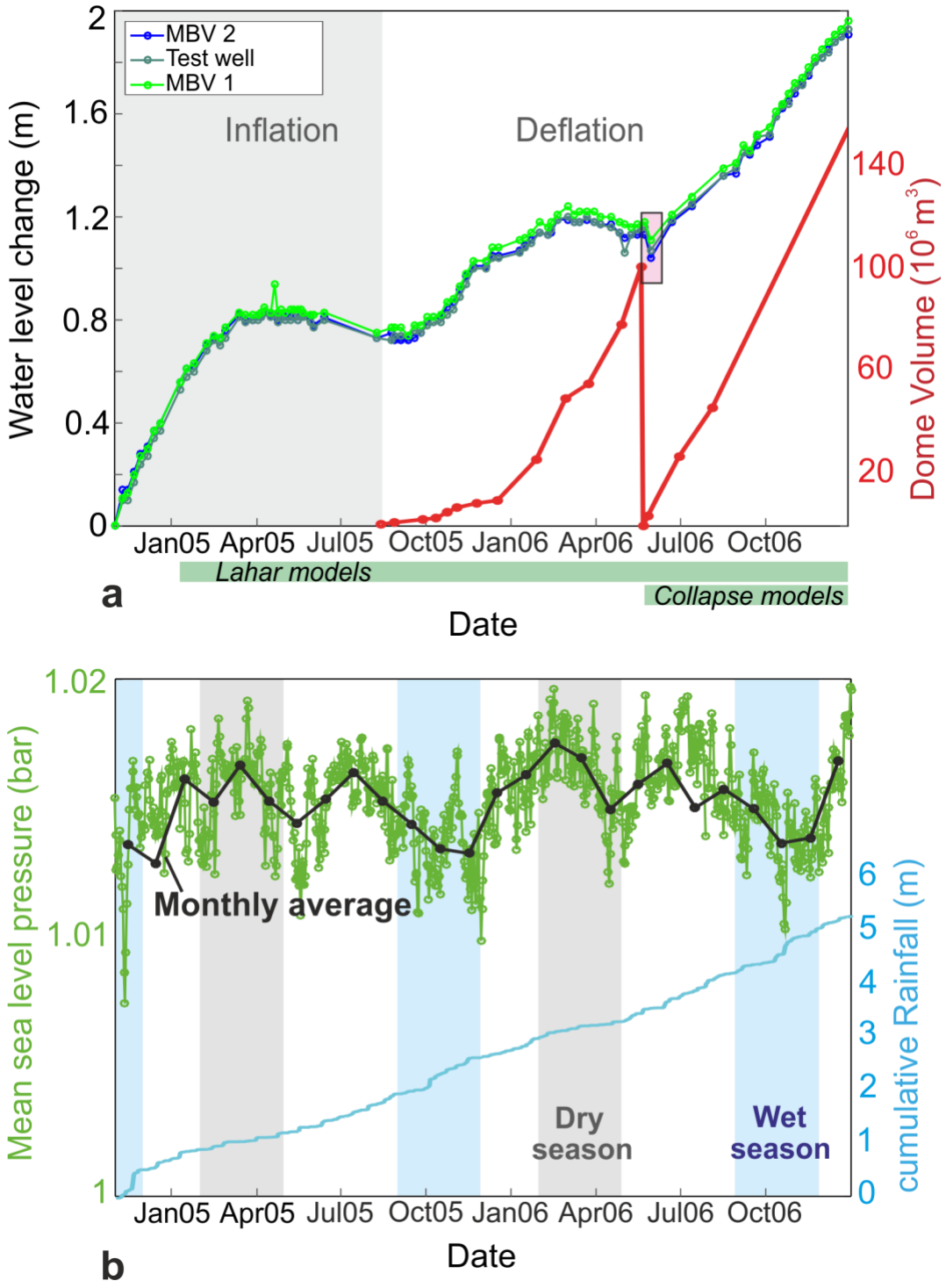

Fig. 2: (a) Water level changes in the three observation wells in the Belham valley (owned by Montserrat Utilities) and dome volume after Ryan et al. (2010). The final depth to water level was 3.87 m for MBV

1, 1.29 m for MBV 2 and 4.7 m for the test well. Water level data can be found in online resource 12. Inflation and deflation-phases of SHV's edifice are indicated, as well as the modelled water level fall in May 2006 (pink box) and the simulation periods for both lahar and collapse models (green boxes). (b) Cumulative rainfall data (owned by Montserrat Utilities, from the Hope rain gauge (see Fig. 1)) and mean sea level pressure at Montserrat's airport (data provided by Karen Pascal, owned by the Government of Montserrat). Rainfall and sea level pressure data can be found in online resource 12. Wet and dry periods are indicated.

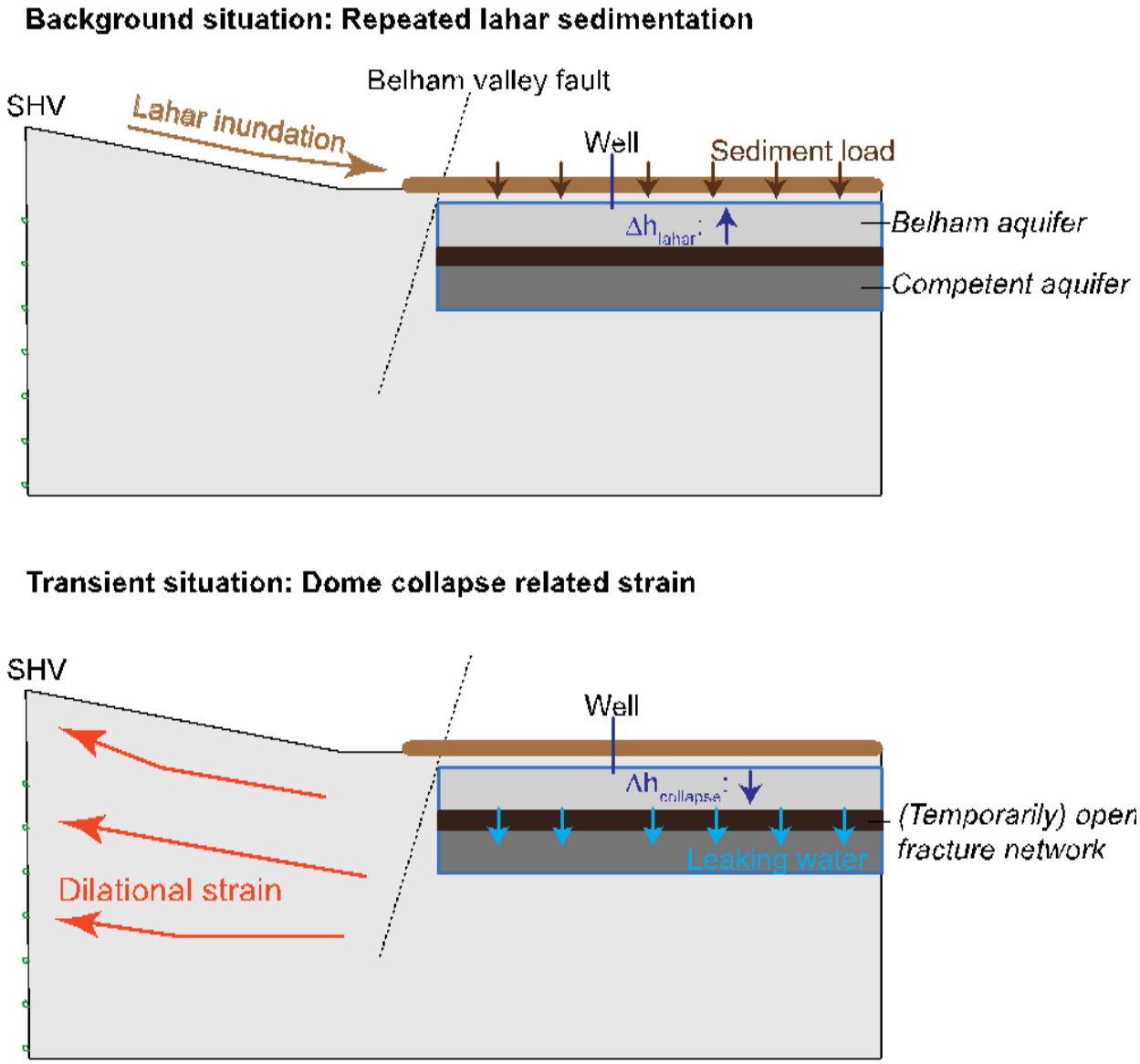

993
994 **Fig. 3**: Conceptual model / hypotheses for hydraulic head changes in the Belham aquifer. The general
995 background situation involves pressure increase in the Belham aquifer due to lahar sedimentation in the
996 valley and a consequent increase in surface load. A transient occurred during the dome collapse, when
997 unloading of the summit and pressure build-up in the UMC led to dilatational strains that caused hydraulic
998 heads to fall significantly in a deeper-seated, competent aquifer. This led to water leaking from the Belham
999 aquifer through a (possibly temporary) fracture network into the deeper system.

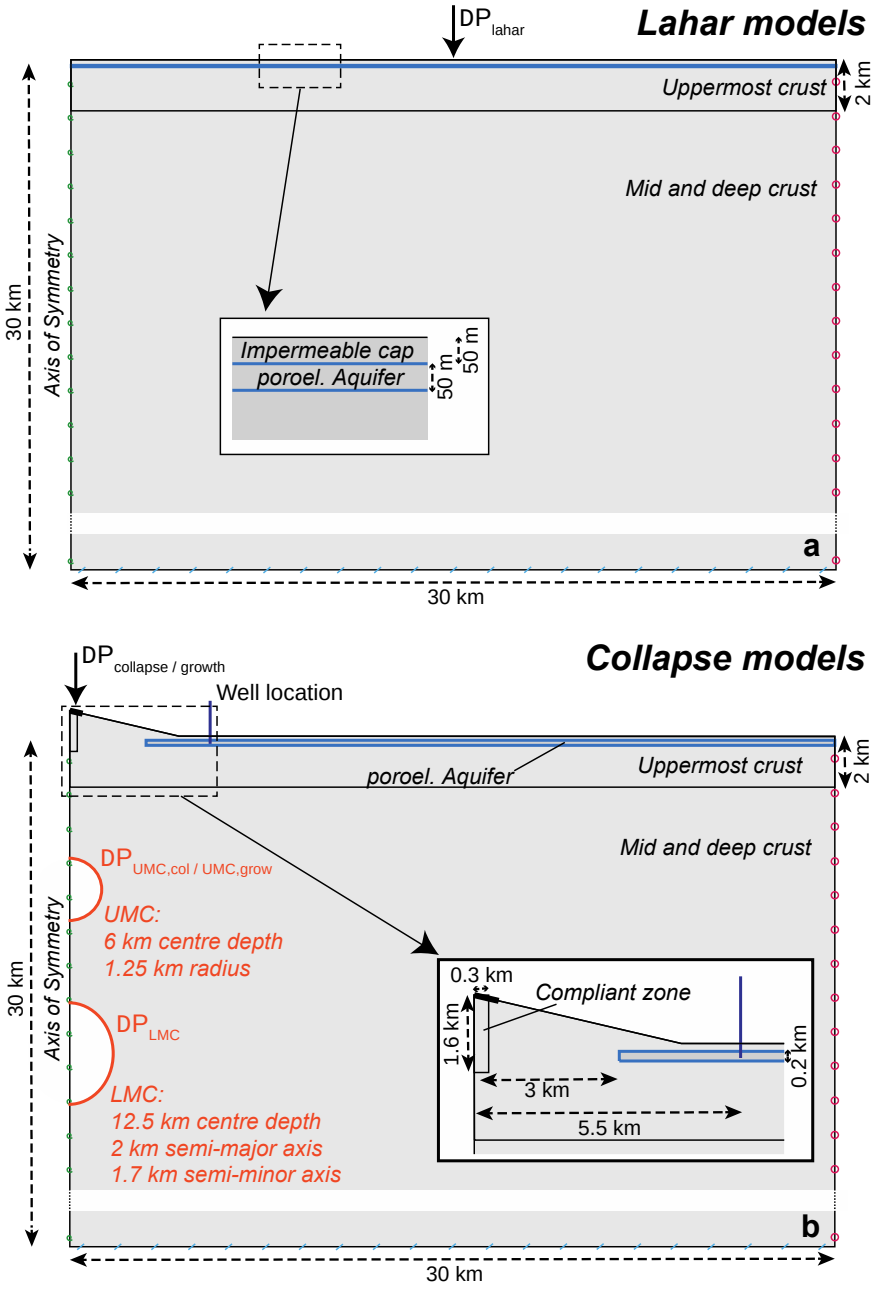

Fig. 4: The lahar (a) and collapse models (b). Topographic height of the summit is 1000 m.a.s.l., radius of the loaded area on the summit is 500 m. Lateral boundary has a roller condition (free lateral, no vertical displacement), bottom boundary is fixed. In (a) the whole surface is loaded according to lahar sedimentation as given in equation 2; in (b), the surface is free. The boundary conditions bordering the aquifer domain are (i) no flow and (ii) continuous stress and displacement. In the dome collapse model, a more compliant zone in the centre of the summit is included with E=0.5 GPa, following Young and Gottsmann (2015). Within

the different layers, material properties are considered isotropic and homogeneous. Groundwater flow is limited to the aquifer domain. Well location in models including topography is indicated in (b). In models without topography, hydraulic head changes are evaluated in the centre of the domain (and are the same everywhere in the model) unless otherwise noted. The magma chambers UMC and LMC are represented by loaded cavities in the domain in (b) (indicated in red).

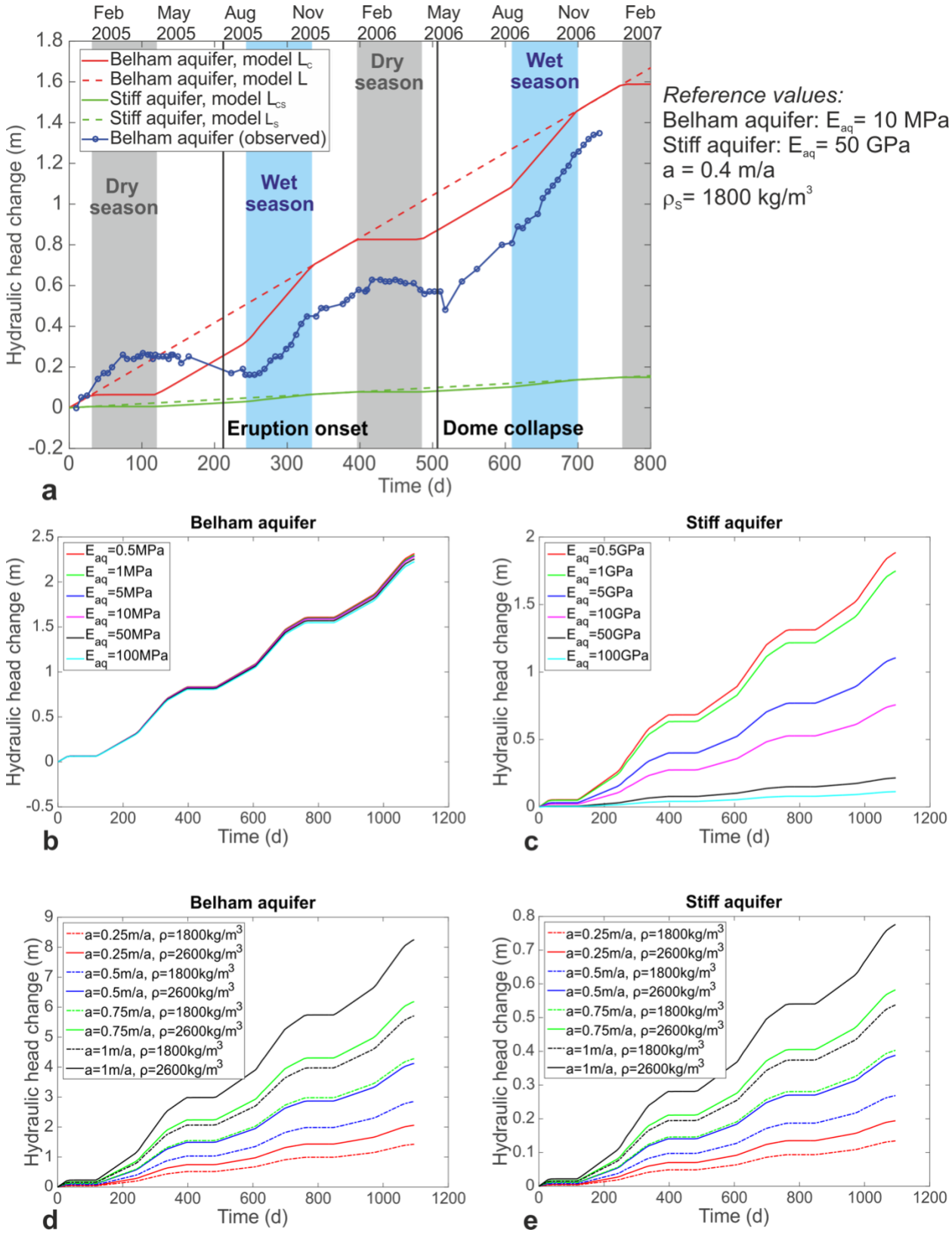
Feb 2005
May 2005
Aug 2005
Nov 2005
Feb 2006
May 2006
Aug 2006
Nov 2006
Feb 2007
Belham aquifer, model L_c
Belham aquifer, model L
Stiff aquifer, model L_{cs}
Stiff aquifer, model L_s
Belham aquifer (observed)
Dry season
Wet season
Dry season
Wet season
Eruption onset
Dome collapse
Hydraulic head change (m)
Time (d)
a
Reference values:
Belham aquifer: E_{aq}= 10 MPa
Stiff aquifer: E_{aq}= 50 GPa
a = 0.4 m/a
ρ_s= 1800 kg/m^3
Belham aquifer
E_{aq}=0.5MPa
E_{aq}=1MPa
E_{aq}=5MPa
E_{aq}=10MPa
E_{aq}=50MPa
E_{aq}=100MPa
Hydraulic head change (m)
Time (d)
b
Stiff aquifer
E_{aq}=0.5GPa
E_{aq}=1GPa
E_{aq}=5GPa
E_{aq}=10GPa
E_{aq}=50GPa
E_{aq}=100GPa
Hydraulic head change (m)
Time (d)
c
Belham aquifer
a=0.25m/a, ρ=1800kg/m^3
a=0.25m/a, ρ=2600kg/m^3
a=0.5m/a, ρ=1800kg/m^3
a=0.5m/a, ρ=2600kg/m^3
a=0.75m/a, ρ=1800kg/m^3
a=0.75m/a, ρ=2600kg/m^3
a=1m/a, ρ=1800kg/m^3
a=1m/a, ρ=2600kg/m^3
Hydraulic head change (m)
Time (d)
d
Stiff aquifer
a=0.25m/a, ρ=1800kg/m^3
a=0.25m/a, ρ=2600kg/m^3
a=0.5m/a, ρ=1800kg/m^3
a=0.5m/a, ρ=2600kg/m^3
a=0.75m/a, ρ=1800kg/m^3
a=0.75m/a, ρ=2600kg/m^3
a=1m/a, ρ=1800kg/m^3
a=1m/a, ρ=2600kg/m^3
Hydraulic head change (m)
Time (d)
e

1020

Fig. 5: (a) Hydraulic head changes with time calculated in different models for a long-term water level rise by sediment loading (both linear and cyclic loading applied to the reference Belham aquifer (models L and L_C) and a stiffer aquifer (models L_{CS} and L_S)), in comparison to observed changes in the water level of MBV 2 from January 2005 onwards. Wet and dry seasons, as well as the timing of eruption onset and dome collapse are indicated. (b)-(e) show results of selected sensitivity studies on Lahar models with cyclic loading: Hydraulic head change with time for a varying Young's Modulus of the aquifer E_{aq} (b, c) and varying sediment density ρ and aggradation a (d, e).

1021

1022

1023

1024

1025

1026

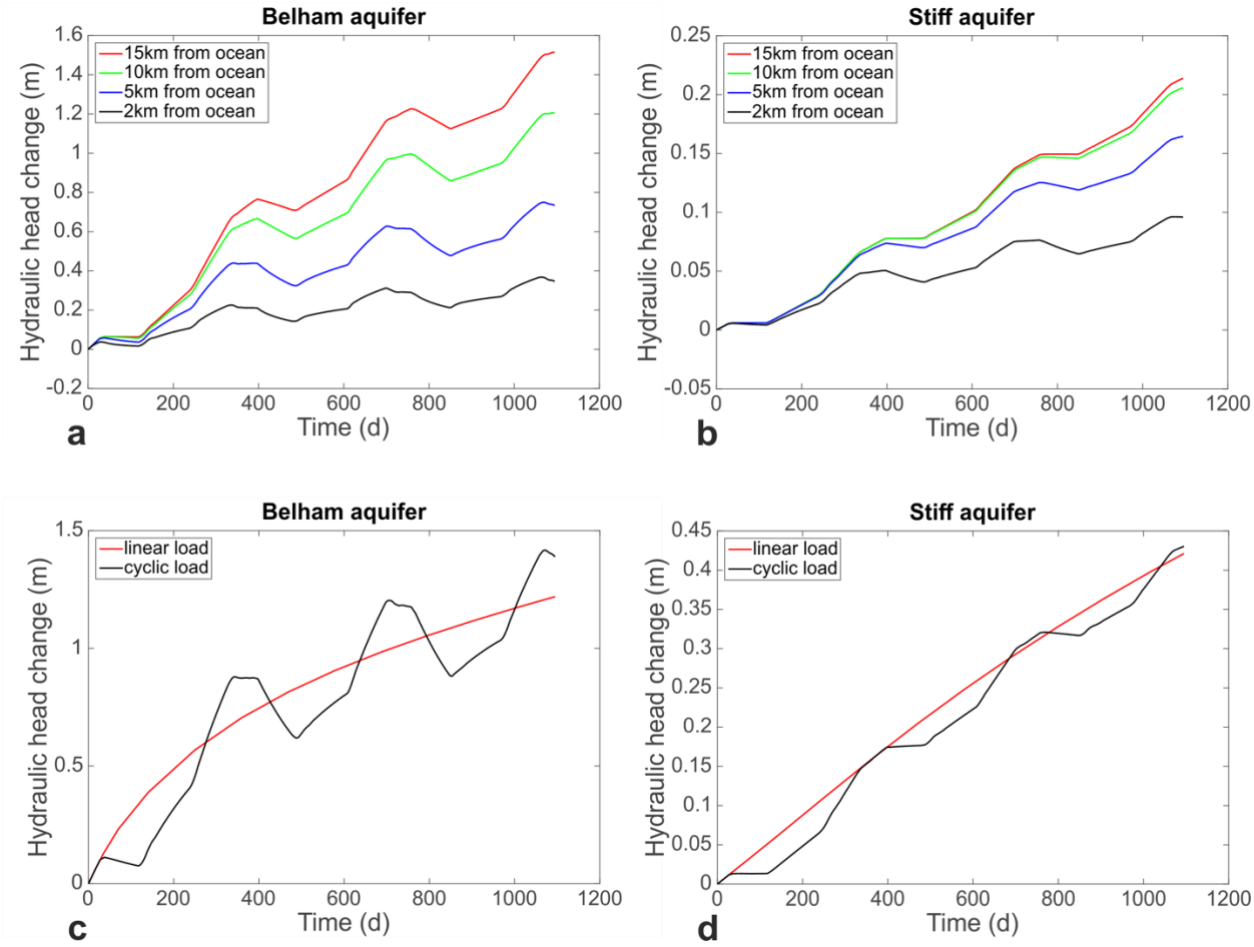

Fig. 6: Results of selected sensitivity studies on Lahar models: Hydraulic head change with time for different distances from the ocean, with a constant water table as lateral boundary condition and cyclic loading (a, b); hydraulic head change with time for topography-dependent surface loading, showing both linear and cyclic loading (c, d).

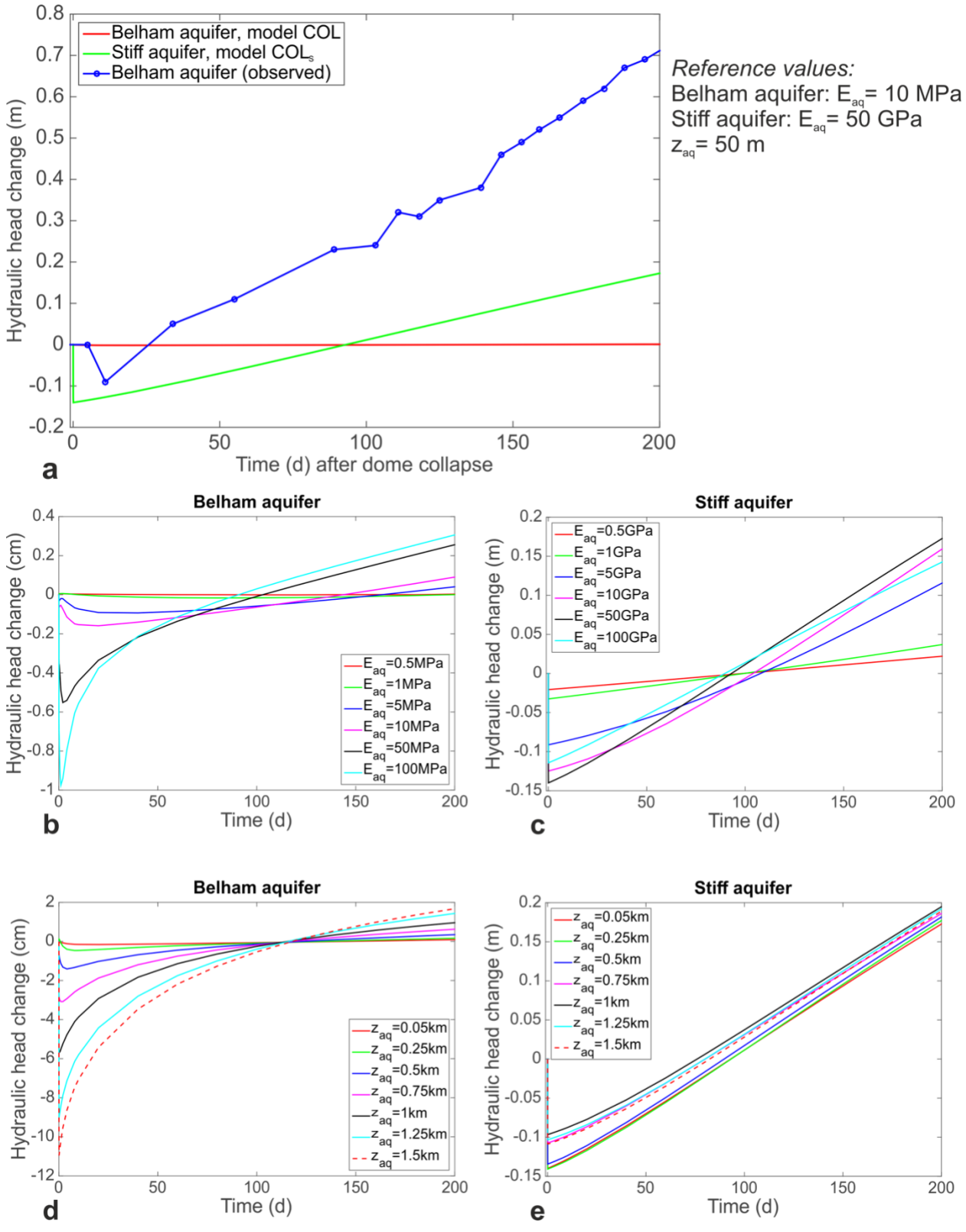
Belham aquifer, model COL
Stiff aquifer, model COL$_s$
Belham aquifer (observed)
Hydraulic head change (m)
Time (d) after dome collapse
a
Reference values:
Belham aquifer: E$_{aq}$= 10 MPa
Stiff aquifer: E$_{aq}$= 50 GPa
z$_{aq}$= 50 m
Belham aquifer
Hydraulic head change (cm)
E$_{aq}$=0.5MPa
E$_{aq}$=1MPa
E$_{aq}$=5MPa
E$_{aq}$=10MPa
E$_{aq}$=50MPa
E$_{aq}$=100MPa
Time (d)
b
Stiff aquifer
Hydraulic head change (m)
E$_{aq}$=0.5GPa
E$_{aq}$=1GPa
E$_{aq}$=5GPa
E$_{aq}$=10GPa
E$_{aq}$=50GPa
E$_{aq}$=100GPa
Time (d)
c
Belham aquifer
Hydraulic head change (cm)
z$_{aq}$=0.05km
z$_{aq}$=0.25km
z$_{aq}$=0.5km
z$_{aq}$=0.75km
z$_{aq}$=1km
z$_{aq}$=1.25km
z$_{aq}$=1.5km
Time (d)
d
Stiff aquifer
Hydraulic head change (m)
z$_{aq}$=0.05km
z$_{aq}$=0.25km
z$_{aq}$=0.5km
z$_{aq}$=0.75km
z$_{aq}$=1km
z$_{aq}$=1.25km
z$_{aq}$=1.5km
Time (d)
e

1036

Fig. 7: (a) Hydraulic head changes with time calculated in models for the water level response to dome growth and collapse (for the reference Belham aquifer (model COL) and a stiffer aquifer (model COLs)), in comparison to observed changes in the water level of MBV 2 from the moment of dome collapse onwards. (b)-(e) show results of selected sensitivity studies: hydraulic head change with time for a varying Young's Modulus of the aquifer E_{aq} (b, c) and aquifer depth z_{aq}.

1037
1038
1039
1040
1041
1042
1043
1044